J. Fluid Mech. (1991), *vol.* 222, *pp.* 369–416
Printed in Great Britain

Three-dimensional distortions of a vortex filament with axial velocity

By YASUHIDE FUKUMOTO[1]† AND TAKESHI MIYAZAKI[2]

[1] Department of Physics, Faculty of Science, University of Tokyo Bunkyo-ku, Tokyo 113, Japan

[2] National Institute for Environmental Studies, Tsukuba, Ibaraki 305, Japan

(Received 13 February 1989 and in revised form 14 June 1990)

Three-dimensional motion of a thin vortex filament with axial velocity, embedded in an inviscid incompressible fluid, is investigated. The deflections of the core centreline are not restricted to be small compared with the core radius. We first derive the equation of the vortex motion, correct to the second order in the ratio of the core radius to that of curvature, by a matching procedure, which recovers the results obtained by Moore & Saffman (1972). An asymptotic formula for the linear dispersion relation is obtained up to the second order. Under the assumption of localized induction, the equation governing the self-induced motion of the vortex is reduced to a nonlinear evolution equation generalizing the localized induction equation. This new equation is equivalent to the Hirota equation which is integrable, including both the nonlinear Schrödinger equation and the modified KdV equation in certain limits. Therefore the new equation is also integrable and the soliton surface approach gives the N-soliton solution, which is identical to that of the localized induction equation if the pertinent dispersion relation is used. Among other exact solutions are a circular helix and a plane curve of Euler's elastica. This local model predicts that, owing to the existence of the axial flow, a certain class of helicoidal vortices become neutrally stable to any small perturbations. The non-local influence of the entire perturbed filament on the linear stability of a helicoidal vortex is explored with the help of the cutoff method valid to the second order, which extends the first-order scheme developed by Widnall (1972). The axial velocity is found to discriminate between right- and left-handed helices and the long-wave instability mode is found to disappear in a certain parameter range when the successive turns of the helix are not too close together. Comparison of the cutoff model with the local model reveals that the non-local induction and the core structure are crucial in making quantitative predictions.

1. Introduction

Vortex tubes, rings and sheets are fundamental elements underlying the dynamics of high-Reynolds-number flows. Since they retain their identities for a long time, a knowledge of the time evolution of vortices is quite helpful in understanding the dynamical structure of real flows.

Concentrated vortices are known to support various fascinating waves. Elongated vortices observed in nature are susceptible to vigorous twisting distortions. Recently Hopfinger, Browand & Gagne (1982), Maxworthy, Mory & Hopfinger (1983) and

† Present address: Department of Applied Physics, Faculty of Engineering, Nagoya University, Chikusa-ku, Nagoya 464-01, Japan.

Maxworthy, Hopfinger & Redekopp (1985) have done elaborate experimental studies of wave motions on vortex cores and revealed the detailed properties of non-axisymmetric and axisymmetric waves.

The maximum radial excursion of the core centreline of the vortices generated by Maxworthy *et al.* (1983, 1985) is comparable with the core radius. In these cases, Leibovich, Brown & Patel (1986, LBP) succeeded in calculating a dispersion relation for bending waves that well approximates the experimental data. They analysed the Howard–Gupta equation (Howard & Gupta 1962) both analytically and numerically for small-amplitude waves on a straight columnar vortex, allowing for axial velocity in the core, and they made headway with respect to a weakly nonlinear theory following Leibovich & Ma (1983). Bending distortions of a vortex filament with large core displacement are also common in nature and are beyond the scope of the weakly nonlinear analysis. Our major concern is the mathematical description of long bending waves on an isolated vortex core whose displacement is not necessarily small compared with the core radius. The fluid is assumed to be inviscid and incompressible.

The strong nonlinearity of the Euler equation has made the full solution for vortex motion inaccessible, so some mathematical idealizations have been unavoidable. The simplest approach is the so-called 'localized induction approximation' put forward by Arms and Hama (Hama, 1962, 1963, Arms & Hama 1965). They assume that the core radius of the vortex tube is so small that the induced velocity at a point on the filament is dominated by the contribution from the neighbouring segment. The resulting equation of motion is referred to as the 'localized induction equation (LIE) and is written as

$$\frac{\partial \boldsymbol{X}}{\partial t} = \frac{\Gamma\kappa}{4\pi}\left[\ln\left(\frac{L}{a}\right)\right]\boldsymbol{b}, \tag{1.1}$$

where $\boldsymbol{X} = \boldsymbol{X}(s,t)$ denotes a point on the filament as a function of the arclength s and the time t, κ is the curvature of the filament curve, $\boldsymbol{b}$ the unit binormal vector, Γ the circulation of the vortex and a the core radius. The remaining parameter L is the length of the segment whose contribution to the induction velocity is taken account of in (1.1). Note that L is indeterminate within the framework of this approximation. Further, neglecting the variation of L/a along the filament and rescaling the time variable, we have

$$\boldsymbol{X}_t = \boldsymbol{X}_s \times \boldsymbol{X}_{ss}, \tag{1.2}$$

where the subscripts indicate the partial differentiation with respect to the indicated variables. Betchov (1965) transformed (1.2) into a coupled system of intrinsic equations for the curvature and torsion with the aid of the Serret–Frenet formulae of space curves. Later, Hasimoto (1972) showed that the LIE is equivalent to the nonlinear Schrödinger equation

$$\mathrm{i}\psi_t + \psi_{ss} + \tfrac{1}{2}|\psi|^2\psi = 0, \tag{1.3}$$

by introducing a complex function

$$\psi = \kappa \exp\left[\mathrm{i}\int^s \tau(s',t)\,\mathrm{d}s'\right]. \tag{1.4}$$

This implies that the LIE is completely integrable and admits soliton excitations. In fact, Hasimoto gave an analytical expression for the 1-soliton solution by reconstructing the space curve from its curvature and torsion corresponding to the 1-soliton solution of nonlinear Schrödinger equation (1.3). This reconstruction

problem, however, is not easy because a highly complex Ricatti equation with the coefficients obtained from knowledge of the curvature and torsion must be solved. Kida (1981) circumvented this obstacle to obtain all the steady shapes of a vortex filament, including a helicoidal filament (Betchov 1965), Euler's elastica (Hasimoto 1971) and the Hasimoto soliton etc., which were essentially described by Kirchhoff's elasastica (Kirchhoff 1859; Hasimoto & Kambe 1985).

Soliton interaction has been studied numerically by Aref & Flinchem (1984) for the collisions of two solitons. Sym (1982, 1984) was the first to develop an analytical approach to solve the inverse problem, which is called the 'soliton surface approach'. According to this approach, solutions of the LIE are expressed in terms of the wave functions of the AKNS equations associated with the nonlinear Schrödinger equation. This geometric approach is then combined with the Darboux transformation to yield the Bäcklund transformation of LIE. Using this, Levi, Sym & Wojciechowski (1983) succeeded in calculating two soliton interactions analytically. Fukomoto & Miyazaki (1986, 1988) adopted the bilinear formalism (Hirota 1982) to obtain the N-soliton solution explicitly. However, a serious problem has arisen in the comparison between the analytical solution and the experimental observations: unfortunately, this solution does not exhibit the clear phase advance during a head-on collision between two solitons shown in the observations by Maxworthy *et al.* (1983, 1985). This discrepancy may be attributed to the several dynamical aspects ignored by the localized induction approximation. For example, Maxworthy *et al.* (1985) pointed out that the cut-off parameter L/a is not a constant but a strong function of the wavenumber or the local curvature.

The stability of helical waves is also of fundamental interest. The study of a helicoidal filament has a long history and all of the existing theoretical studies conclude that it is unstable to infinitesimal perturbations (Levy & Forsdyke 1928; Betchov 1965; Widnall 1972: Kida 1981, 1982). However, Maxworthy *et al.* (1985) reported that helical waves are observed to exist stably for some time. Although the observed wave amplitude is not large, this result leads us to the expectation that there might be stable helical waves of finite amplitude if some mechanisms were incorporated into the stability analysis.

These considerations inspired us to explore the hidden dynamical effects. A salient feature of the formation of concentrated vortices is the inclusion of strong axial flow in vortex cores, different from the surrounding flow. Tornadoes, bath-plug vortices and trailing vortices behind the wing of an aircraft are the typical examples. The magnitude of the axial velocity near the core axis was substantial in the laboratory experiments by Maxworthy *et al.* (1983, 1985). The principle aim of the present paper is to shed light on the effect of axial flow upon the large-amplitude long bending waves of a slender vortex tube.

If we assume that the core radius is very small in comparison with the local radius of curvature, we can use the method of matched asymptotic expansions to determine the self-induced velocity of the vortex. Widnall, Bliss & Zalay (1971) calculated the velocity up to $O(\Gamma/R)$, permitting arbitrary axisymmetric distributions of the swirl and axial velocities. Here R is a measure of the radius of curvature. This result was generalized by Callegari & Ting (1978) to include the viscous diffusion of the vorticity with a particular initial distribution. Considering the force balance at the edge of the vortex core, Moore & Saffman (1972) derived the inviscid equation of motion correct to $O(\Gamma a/R^2)$, i.e. to second order. Their derivation is based on compact and elegant physical intuition and we think that it is worth deriving it in a more straightforward and systematic manner.

In §2 we present the derivation of the Moore–Saffman filament equation by making use of the method of matched asymptotic expansions up to the second order. The second-order correction to the linear dispersion relation for helical waves on a straight columnar vortex is deduced.

In §3.1 we demonstrate that, under assumptions similar to those of the localized induction approximation, the Moore–Saffman equation can be simplified to a new integrable nonlinear evolution equation. The new equation is equivalent to the Hirota (1973) equation which includes both the nonlinear Schrödinger equation and the modified KdV equation. The N-soliton solution is obtainable through the soliton surface approach and Hirota's bilinear method (Miyazaki & Fukumoto 1988), which is described in §3.2. Some other exact solutions including Euler's elastica and a helicoidal filament are collected in §3.3. In §3.4 we study the linear stability of a helicoidal filament on the basis of our new model equation. There, the stabilizing or destabilizing effect of the axial velocity upon the long-wave disturbances on a helicoidal filament is clarified. A novel feature is the existence of a class of stable helicoidal filaments.

There are, however, some problematical steps in the passage from the full Moore–Saffman equation to its local-induction version. This ambiguity motivates us to investigate the influence of the entire perturbed filament on the stability of a helicoidal filament. One reliable and feasible approach to this is the 'cutoff' method proposed by Crow (1970) and refined by Widnall *et al.* (1971) and Moore & Saffman (1972). Widnall (1972) applied this method to study the stability of a helicoidal vortex filament, which is valid to the first order. In §4, we study the same problem by extending Widnall's procedure to the second order on the basis of the Moore–Saffman equation. The results of the local model in §3.4 are then assessed and the axial-flow effect on the long-wave and other modes of a helicoid is elucidated over a wide range of the geometric parameters.

The last section (§5) is devoted to a summary and conclusions.

2. The self-induced motion of a thin vortex filament

In this section we shall derive a closed system of equations for the self-induced velocity of a thin vortex filament with axial flow in the core, up to the second order with respect to the curvature effect. We begin with the evaluation of the Biot–Savart integral.

2.1. *Biot–Savart formula*

Let us recall the kinematical result for an incompressible fluid that, once the solenoidal distribution of vorticity is specified at all points of the fluid together with the boundary conditions on the velocity, the velocity of the fluid is determined uniquely over the entire fluid region. Without any boundary, the fluid velocity $\boldsymbol{v}(\boldsymbol{x})$ at a point $\boldsymbol{x}$ is connected to the vorticity distribution $\boldsymbol{\omega}(\boldsymbol{x})$ by the Biot–Savart law:

$$\boldsymbol{v}(\boldsymbol{x}) = -\frac{1}{4\pi}\int \mathrm{d}^3\boldsymbol{x}'\boldsymbol{\omega}(\boldsymbol{x}')\times\nabla\frac{1}{|\boldsymbol{x}-\boldsymbol{x}'|}. \tag{2.1}$$

An axial-velocity distribution inside the vortex core gives rise to the transverse as well as the axial vorticity component. We assume that both the axial and transverse components of vorticity are confined to a thin core region and that the core radius a is much smaller than the local radius of curvature of the vortex filament R. In the following, we calculate the induction velocity near the vortex core due to these two components of vorticity separately.

To this end, we introduce an orthonormal curvilinear coordinate system attached to each point $\boldsymbol{X}(s,t)$ on the filament, which is the same as that employed by Widnall *et al.* (1971). Moore & Saffman (1972) and Callegari & Ting (1978). For any point $\boldsymbol{x}$ close to the vortex core the corresponding nearest point $\boldsymbol{X}(s,t)$ on the filament can be chosen, uniquely. We define local cylindrical coordinates (r,θ,s) centred on $\boldsymbol{X}(s,t)$ in the following way. The position on the plane containing the normal vector $\boldsymbol{n}$ and the binormal vector $\boldsymbol{b}$ at $\boldsymbol{X}(s,t)$ is specified by the r- and θ-coordinates. Let us take the angle φ so that $\boldsymbol{n}$ makes angle φ (and $\boldsymbol{b}$ makes $\pi/2-\varphi$) with the unit vector $\boldsymbol{e}_r$ in the radial direction. Then we can get a set of orthogonal coordinates if the angle θ is defined by

$$\theta = \varphi - \theta_0(s,t), \tag{2.2}$$

where

$$\frac{\partial \theta_0}{\partial s} = -\tau. \tag{2.3}$$

In this coordinate system the position vector $\boldsymbol{x}$ is given by

$$\boldsymbol{x} = \boldsymbol{X}(s,t) + r\boldsymbol{e}_r. \tag{2.4}$$

We can check that this toroidal system is indeed orthogonal, namely

$$\mathrm{d}\boldsymbol{x} = \boldsymbol{e}_r\,\mathrm{d}r + r\boldsymbol{e}_\theta\,\mathrm{d}\theta + h\boldsymbol{t}\,\mathrm{d}s, \tag{2.5}$$

where

$$h = 1-\kappa r\cos\varphi, \tag{2.6}$$

and $\boldsymbol{e}_\theta$ denotes the unit azimuthal vector. In order for the local system to be well defined, the region described by each local system about a point on the vorticity centroid has to be limited to the distance $O(R)$ from that point.

First we write down the known results for the induced velocity caused by the axial vorticity and denote it by $\boldsymbol{v}_1$. Under the condition that the vortex is very thin, the volume integral in (2.1) may be replaced by a line integral,

$$\boldsymbol{v}_1 = -\frac{\Gamma}{4\pi}\int \frac{(\boldsymbol{x}-\boldsymbol{X}')\times \boldsymbol{t}'}{|\boldsymbol{x}-\boldsymbol{X}'|^3}\,\mathrm{d}s', \tag{2.7}$$

where $\boldsymbol{X}'(s',t')$ denotes the position vector of a point on the filament curve. When we calculate the velocity near the vortex core, the contribution of the local portion dominates the Biot–Savart integral (2.7). The Taylor expansion of $\boldsymbol{X}'$ in the arclength s' around the point $\boldsymbol{X}(s,t)$ nearest to the given fluid position $\boldsymbol{x}$ is, to cubic order,

$$\boldsymbol{X}'(s',t) = \boldsymbol{X}(s,t) + \boldsymbol{t}(s'-s) + \tfrac{1}{2}\kappa\boldsymbol{n}(s'-s)^2 + \frac{1}{3!}(-\kappa^2\boldsymbol{t} + \kappa_s\boldsymbol{n} + \kappa\tau\boldsymbol{b})(s'-s)^3 + O[(s'-s)^4]. \tag{2.8}$$

Inserting (2.8) into (2.7) and integrating along the filament over a distance L on either side of the point s, we obtain, in the limit $a \ll r \ll R$,

$$\boldsymbol{v}_1 = \frac{\Gamma}{2\pi r}\boldsymbol{e}_\theta + \frac{\Gamma\kappa}{4\pi}\left[\ln\left(\frac{2L}{r}\right)-1\right]\boldsymbol{b} + \frac{\Gamma\kappa}{4\pi}\cos\varphi\,\boldsymbol{e}_\theta + \frac{3\Gamma\kappa^2 r}{16\pi}\left\{(\boldsymbol{e}_r\sin 2\varphi + \boldsymbol{e}_\theta\cos 2\varphi)\left[\ln\left(\frac{2L}{r}\right)-\frac{4}{3}\right] + \tfrac{1}{2}\cos 2\varphi\,\boldsymbol{e}_\theta + \tfrac{1}{18}\boldsymbol{e}_\theta\right\} + \boldsymbol{Q} + O\left(\frac{\Gamma a^2}{R^3}\right), \tag{2.9}$$

where $\boldsymbol{Q}$ is the remaining non-local contribution to the integral. (See Moore & Saffman 1972; Callegari & Ting 1978 for details.)

Next, we evaluate the contribution due to the transverse vorticity component $\omega_T(n)$ in (2.1). It is assumed that the vortex lines of the transverse vorticity constitute a set of closed contours $C(n)$ in a given cross-sectional plane and that n is taken to be the orthogonal coordinate to those contours. In this case (2.1) is reduced to

$$v_2 = -\frac{1}{4\pi}\int ds' \int\left[\omega_T(n)\int_{C(n)} \delta l' \times \nabla \frac{1}{|x-x'|}\right] dn, \tag{2.10}$$

where $\delta l'$ is a length increment along the direction of a transverse vortex line on $C(n)$. With the help of Stokes' theorem, (2.10) becomes

$$v_2 = -\frac{1}{4\pi}\int ds' \int\left\{\omega_T(n)\int_{S(n)}\left[(t'\times\nabla')\times\nabla\frac{1}{|x-x'|}\right]dS'\right\}\delta n \tag{2.11}$$

$$= \int ds' \int\left\{\omega_T(n)\left[\int_{S(n)} t'\delta(x-x')\,dS'\right]\delta n\right\}$$

$$+\frac{1}{4\pi}\int ds' \int\left[\omega_T(n)\left\{\int_{S(n)}\left[\frac{3(x-x')\,(x-x')\cdot t'}{|x-x'|^5}-\frac{t'}{|x-x'|^3}\right]dS'\right\}\delta n\right], \tag{2.12}$$

where $S(n)$ indicates the surface enclosed by the contour $C(n)$ and t' is the unit normal vector to that surface. We postulate that the velocity component in the normal direction parametrized by n is absent and that the other components of velocity depend only on n and t. Then, the transverse vorticity is expressed by

$$\omega_T = -\frac{\partial w^{(0)}}{\partial n}. \tag{2.13}$$

Substituting (2.13) into (2.12), we have, after partial integration,

$$v_2 = \int ds'\left[\int_{S(\infty)} w^{(0)}(n,t)\,t'\delta(x-x')\,dS'\right]$$

$$-\frac{1}{4\pi}\nabla\int ds'\left[\int_{S(\infty)} w^{(0)}(n,t)\frac{(x-x')\cdot t'}{|x-x'|^3}dS'\right]. \tag{2.14}$$

The first term is simply the axial flow inside the core. The second term means that the distribution of the transverse vorticity is replaced by that of doublets. It is the second term that is directly related to the induction velocity outside the core. This result corresponds to the familiar fact that the flow field induced by a vortex ring is equivalent to that due to a system of doublets distributed with uniform density over the interior of the circle and that the transverse vorticity may be regarded as the sum of a series of vortex rings. If the axial velocity has significant values only within a thin core, which is the case we are concerned with, the second term on the right-hand side of (2.14) is reduced to

$$v_2 = -\frac{1}{4\pi}\left[\int_{S(\infty)} w^{(0)}\,dS'\right]\nabla\int\frac{(x-X')\cdot t'}{|x-X'|^3}ds' \tag{2.15}$$

in the irrotational region outside the vortex core. The integration of (2.15) can be performed along the entire arrlength s' as follows:

$$v_2 = -\frac{1}{4\pi}\left[\int_{S(\infty)} w^{(0)}\,dS'\right]\nabla\int ds'\left(\frac{\partial}{\partial s'}\frac{1}{|x-X'|}\right)$$

$$= 0. \tag{2.16}$$

Thus, the distribution of doublets along the filament makes no contribution to the induced velocity, which is equivalent to the statement that the magnetic field of a long thin coil is confined to the core. The contribution to the Biot–Savart integral is due, solely, to the axial-vorticity distribution, whose evaluation has been completed by (2.9) However, it turns out that the extrapolation of (2.9) to the surface of the vortex tube is insufficient to evaluate the velocity of the vortex filament. We need a detailed knowledge of the flow field in the vicinity of the vortex core, where the coupling between the axial and azimuthal vorticity components plays an essential role. Equation (2.9) provides us only with the limiting form of the outer flow field applicable to the region closer to the core, but not in the immediate neighbourhood.

In the remainder of this section, we inquire into the solution of the Euler equation valid within and near the vortex core by using a perturbation technique up to the second order in the ratio of the core radius to that of curvature. Thereafter the resulting near field is matched to the outer flow given by (2.9) to yield the velocity of the vortex filament.

2.2. *The inner and outer expansions*

Widnall *et al.* (1971) and Callegari & Ting (1978) have already given the first-order correction term using a matching method. The latter generalizes the former to take account of viscous decay of the vortex core. We make an attempt at a straightforward extension of the matching technique to the second order, though we confine ourselves to the inviscid core dynamics. First, we adapt their expansion scheme for our purpose.

Suppose that the space curve $\boldsymbol{X}(s,t)$ is the centroid of the axial-vorticity distribution in each core cross-section. In addition we require that the curve $\boldsymbol{X}$ moves as a material line so that it is always composed of the same fluid particles. Here we introduce a marker variable ξ along the curve satisfying the condition

$$\dot{\boldsymbol{X}}\cdot\boldsymbol{t} = \boldsymbol{Q}\cdot\boldsymbol{t} = Q_{\parallel}, \tag{2.17}$$

and occasionally use it in place of s when convenient. Here $\dot{\boldsymbol{X}}$ is the velocity of a point on the curve specified by ξ:

$$\dot{\boldsymbol{X}} = \frac{\partial \boldsymbol{X}}{\partial t}(\xi, t). \tag{2.18}$$

Then the above conditions read

$$\dot{\boldsymbol{X}}\cdot\boldsymbol{n} = \boldsymbol{v}\cdot\boldsymbol{n}, \quad \dot{\boldsymbol{X}}\cdot\boldsymbol{b} = \boldsymbol{v}\cdot\boldsymbol{b} \quad \text{at} \quad r = 0, \tag{2.19}$$

where $\boldsymbol{v}$ is the total velocity of the fluid in a rest frame.

In order to perform the matched asymptotic expansions, it is convenient to rewrite the equations of motion in dimensionless form. We have two typical lengthscales: one a measure of the core radius a_0 and the other that of the radius of curvature R_0 of the curve $\boldsymbol{X}(s,t)$, and their ratio is denoted by ϵ:

$$\epsilon = \frac{a_0}{R_0}. \tag{2.20}$$

Generally, owing to the vortex-line stretching, the core radius a depends on both t and s. The typical choice of a_0 is the core radius of the initial unperturbed vortex, which is assumed to be uniform along the arclength. We shall seek the solution as expansions in powers of ϵ under the requirement

$$\epsilon \ll 1. \tag{2.21}$$

Let us assume that the lengthscale of significant variation along the vortex filament is $O(R_0)$ and normalize the arclength, $\boldsymbol{X}'$ and the local radius of curvature by R_0:

$$s = s'/R_0, \quad \xi = \xi'/R_0, \quad \boldsymbol{X} = \boldsymbol{X}'/R_0, \quad R = R'/R_0. \tag{2.22}$$

Here as a tentative notation we distinguish each dimensional quantity by attaching a prime to the corresponding dimensionless variable. For the outer expansions valid at large distances from the vortex tube, the appropriate normalization of the radial coordinate is

$$\tilde{r} = r'/R_0. \tag{2.23}$$

The inner expansions are valid in the neighbourhood of the core and the dimensionless inner radial variable is defined as

$$r = r'/a_0 = \tilde{r}/\epsilon. \tag{2.24}$$

We anticipate that the vortex evolves mainly according to the LIE (1.1). In such a case the time variable is non-dimensionalized as

$$t = t' \Big/ \left(\frac{2\pi R_0^2}{\Gamma}\right), \tag{2.25}$$

which implies that we focus our attention on rather slow bending modes. The velocity and the pressure p are non-dimensionalized using the maximum swirl velocity:

$$\boldsymbol{v} = \boldsymbol{v}' \Big/ \left(\frac{\Gamma}{2\pi a_0}\right), \quad p = p' \Big/ \left[\rho_0 \left(\frac{\Gamma}{2\pi a_0}\right)^2\right]. \tag{2.26}$$

Here ρ_0 is the density of the fluid.

The outer solution is constructed by evaluating the Biot–Savart integral with the vortex tube regarded as a space curve. The asymptotic behaviour of the solution in the intermediate region (the overlap domain) is provided by (2.9). Equation (2.9), in turn, plays the part of the matching condition, i.e. the boundary condition imposed on the inner solution at infinity.

In order to obtain the inner solution, it is advantageous to work in the moving cylindrical coordinates (r, θ, s), already mentioned. Let $\boldsymbol{V} = (u, v, w)$ denote the velocity in this coordinate system. Then the fluid velocity as seen in a fixed coordinate system is written in terms of the dimensionless variables as

$$\boldsymbol{v}(r, \theta, s, t) = \epsilon \dot{\boldsymbol{X}} + \boldsymbol{V}(r, \theta, s, t). \tag{2.27}$$

The full equations of motion in the moving system are contained in the Appendix. Suppose that the form of the curve $\boldsymbol{X}(s, t)$ is specified over the entire range of the length parameter at some instant. We search for the solution in the form of series expansions in ϵ. We observe that the term proportional to $\ln \epsilon$ inevitably appears, in view of the nature of the Biot–Savart integral. We take into account this dependence implicitly as that of the coefficients in the ϵ-expansions.

Thus we proceed by postulating the following forms of inner expansions for the velocity and the pressure:

$$u = \epsilon u^{(1)}(r, \theta, s, t) + \epsilon^2 u^{(2)}(r, \theta, s, t) + \ldots, \tag{2.28}$$

$$v = v^{(0)}(r, t) + \epsilon v^{(1)}(r, \theta, s, t) + \epsilon^2 v^{(2)}(r, \theta, s, t) + \ldots, \tag{2.29}$$

$$w = w^{(0)}(r, t) + \epsilon w^{(1)}(r, \theta, s, t) + \epsilon^2 w^{(2)}(r, \theta, s, t) + \ldots, \tag{2.30}$$

$$p = p^{(0)}(r, t) + \epsilon p^{(1)}(r, \theta, s, t) + \epsilon^2 p^{(2)}(r, \theta, s, t) + \ldots, \tag{2.31}$$

$$\dot{\boldsymbol{X}} = \dot{\boldsymbol{X}}^{(0)}(\xi, t) + \epsilon \dot{\boldsymbol{X}}^{(1)}(\xi, t) + \ldots. \tag{2.32}$$

The leading-order velocity corresponding to the unperturbed straight vortex has swirl and axial components only. We require that these components do not depend on θ and s. The time dependence follows from the vortex-line stretching which is uniform with respect to s. The non-uniform stretching is shown to have no influence on the leading-order velocity. Then we can easily confirm that the Euler equations for the leading terms are satisfied.

According to (2.19), the boundary conditions at the centroid $\boldsymbol{X}$ of the vortex are

$$u = v = 0 \quad \text{at} \quad r = 0. \tag{2.33}$$

The remaining conditions are the requirement that the outer and inner solutions be matched to each other. We assume that the velocity is smoothly continuous across the core boundary, following Callegari & Ting. In this case, if the velocity in the inner regime is connected continuously with that in the outer regime, then the continuity of the pressure is automatically insured. Rewriting (2.9) in terms of the dimensionless (inner) variables, the matching condition as $r \to \infty$ reads

$$v^{(0)} \sim \frac{1}{r} + o(r^{-n}), \quad w^{(0)} \sim o(r^{-n}) \quad \text{for} \quad n = 2, \tag{2.34}$$

$$u^{(1)} \sim \tfrac{1}{2}\kappa\left[\ln\left(\frac{2\tilde{L}}{\epsilon r}\right) - 1\right]\sin\varphi + [\boldsymbol{Q}^{(1)} - \dot{\boldsymbol{X}}^{(0)}]\cdot\boldsymbol{e}_r, \tag{2.35a}$$

$$v^{(1)} \sim \tfrac{1}{2}\kappa\left[\ln\left(\frac{2\tilde{L}}{\epsilon r}\right) - 1\right]\cos\varphi + \tfrac{1}{2}\kappa\cos\varphi + [\boldsymbol{Q}^{(1)} - \dot{\boldsymbol{X}}^{(0)}]\cdot\boldsymbol{e}_\theta, \tag{2.35b}$$

$$u^{(2)} \sim \tfrac{3}{8}\kappa^2 r\left[\ln\left(\frac{2\tilde{L}}{\epsilon r}\right) - \frac{4}{3}\right]\sin 2\varphi + [\boldsymbol{Q}^{(2)} - \dot{\boldsymbol{X}}^{(1)}]\cdot\boldsymbol{e}_r, \tag{2.36a}$$

$$v^{(2)} \sim \tfrac{3}{8}\kappa^2 r\left[\ln\left(\frac{2\tilde{L}}{\epsilon r}\right) - \frac{5}{6}\right]\cos 2\varphi + \frac{\kappa^2 r}{48} + [\boldsymbol{Q}^{(2)} - \dot{\boldsymbol{X}}^{(1)}]\cdot\boldsymbol{e}_\theta, \tag{2.36b}$$

where $\tilde{L} = L/R_0$.

The solution for the axial velocity will prove to be unnecessary for the final determination of the velocity of the vortex.

2.3. *The inner solution and the velocity of a vortex filament*

Before calculating the second-order perturbations, we present a brief review of the first-order perturbations in the inner region. At first order the equations of motion take the following forms (see the Appendix):

$$\frac{v^{(0)}u_\theta^{(1)}}{r} - \frac{2v^{(0)}v^{(1)}}{r} + \kappa[w^{(0)}]^2\cos\varphi = -p_r^{(1)}, \tag{2.37}$$

$$v_r^{(0)}u^{(1)} + \frac{v^{(0)}v_\theta^{(1)}}{r} + \frac{v^{(0)}u^{(1)}}{r} - \kappa[w^{(0)}]^2\sin\varphi = -\frac{p_\theta^{(1)}}{r}, \tag{2.38}$$

$$u^{(1)}w_r^{(0)} + \frac{v^{(0)}w_\theta^{(1)}}{r} + \kappa w^{(0)}v^{(0)}\sin\varphi = 0, \tag{2.39}$$

where use has been made of the assumption that the leading-order velocity is axisymmetric and uniform along the vortex filament. The equation of continuity is

$$v_\theta^{(1)} + [ru^{(1)}]_r + \kappa r v^{(0)}\sin\varphi = 0. \tag{2.40}$$

Equation (2.40) is satisfied by introducing a stream function related to the cross-sectional velocity by

$$u^{(1)} = \frac{1}{r}\psi_\theta^{(1)}, \quad v^{(1)} = -\psi_r^{(1)} + \kappa r v^{(0)} \cos\varphi. \tag{2.41}$$

Eliminating the pressure $p^{(1)}$ from (2.37) and (2.38) and making use of (2.41), we have

$$\left(\nabla^2 - \frac{\zeta_r^{(0)}}{v^{(0)}}\right)\psi_\theta^{(1)} = -\kappa \sin\varphi \left[2r\zeta^{(0)} + v^{(0)} + \frac{2rw^{(0)}w_r^{(0)}}{v^{(0)}}\right], \tag{2.42}$$

where

$$\zeta^{(0)} = \frac{1}{r}[rv^{(0)}]_r \tag{2.43}$$

is the axial-vorticity component and ∇^2 is the two-dimensional Laplacian:

$$\nabla^2 = \frac{\partial^2}{\partial r^2} + \frac{1}{r}\frac{\partial}{\partial r} + \frac{1}{r^2}\frac{\partial^2}{\partial \theta^2}. \tag{2.44}$$

The boundary conditions (2.33) are, at the present order,

$$\frac{1}{r}\psi_\theta^{(1)} = \psi_r^{(1)} = 0 \quad \text{at} \quad r = 0. \tag{2.45}$$

By inspection, we readily find that the appropriate form of the solution is

$$\psi^{(1)} = \hat{\psi}_0^{(1)}(r, s, t) + \hat{\psi}^{(1)}(r, s, t)\cos\varphi. \tag{2.46}$$

Substitution of (2.46) into (2.42) yields

$$\hat{\mathrm{L}}\hat{\psi}^{(1)} = \kappa\left[2r\zeta^{(0)} + v^{(0)} + \frac{2rw^{(0)}w_r^{(0)}}{v^{(0)}}\right], \tag{2.47}$$

where

$$\hat{\mathrm{L}} = \frac{\partial^2}{\partial r^2} + \frac{1}{r}\frac{\partial}{\partial r} - \left(\frac{1}{r^2} + \frac{\zeta_r^{(0)}}{v^{(0)}}\right). \tag{2.48}$$

Notice that no equation governing $\hat{\psi}_0^{(1)}$ is available. This axisymmetric part of the stream function gives the axisymmetric part of the first-order swirl velocity. We suppress this term by postulating the following expansion form for the dimensional core radius a:

$$a(s, t) = a(t) + \epsilon^2 a^{(2)}(s, t). \tag{2.49}$$

This is really a hypothesis, because the construction of $\hat{\psi}_0^{(1)}$ requires the solution of the third-order perturbations. Moore & Saffman (1972) gave a physical argument for it based on fast core-area waves of velocity of $O(\Gamma/a)$, which would quickly smooth out any non-uniformity in the core radius. Recently Lundgren & Ashurst (1989) proposed a model equation incorporating the fast area-varying waves on a vortex core and developed a nonlinear theory of helical as well as axisymmetric waves. This hypothesis, together with the conservation of circulation associated with the axial vorticity, leads us to the conclusion that the corrections to the axisymmetric part appear at higher orders. One of the homogeneous solutions of (2.47) is found to be $v^{(0)}$.

We can then build the general solution of (2.47) subject to the boundary condition (2.45) at $r = 0$ as follows:

$$\hat{\psi}^{(1)} = \kappa v^{(0)} \int_0^r \frac{\mathrm{d}z}{z[v^{(0)}(z)]^2} \left\{ \int_0^z \eta[2\eta v^{(0)}\zeta^{(0)} + (v^{(0)})^2 + 2\eta w^{(0)} w_\eta^{(0)}]\,\mathrm{d}\eta \right\}. \tag{2.50}$$

Now we are in a position to match the inner field to the outer one. The matching condition (2.35), when expressed in terms of the stream function, is

$$\psi^{(1)} \sim -\tfrac{1}{2}\kappa r\cos\varphi \left[\ln\left(\frac{2\tilde{L}}{\epsilon r}\right) - 1\right] + r(\boldsymbol{Q}^{(1)} - \dot{\boldsymbol{X}}^{(0)}) \cdot (\boldsymbol{n}\sin\varphi - \boldsymbol{b}\cos\varphi) \quad \text{as} \quad r \to \infty. \tag{2.51}$$

The asymptotic behaviour of (2.50) at large values of r is found by returning to (2.47), together with (2.34), as

$$\hat{\psi}^{(1)} \sim \tfrac{1}{2}\kappa r \ln r + rA + O\left(\frac{1}{r}\right), \tag{2.52}$$

where $A = A(s,t)$ is a function obtainable from (2.50). Remembering the definition (2.46) supplemented by the condition $\hat{\psi}_0^{(1)} = 0$, we conclude that the matching condition is achieved by requiring that

$$\dot{\boldsymbol{X}}^{(0)} = \left\{ \tfrac{1}{2}\kappa \left[\ln\left(\frac{2\tilde{L}}{\epsilon}\right) - 1\right] + A(s,t) \right\} \boldsymbol{b} + \boldsymbol{Q}^{(1)}. \tag{2.53}$$

Comparison of (2.50) with (2.52) produces

$$A = \kappa \lim_{r\to\infty} \left[\frac{v^{(0)}}{r} \int_0^r \frac{\mathrm{d}z}{z[v^{(0)}]^2} \left\{ \int_0^z \eta[2\eta v^{(0)}\zeta^{(0)} + (v^{(0)})^2 + 2\eta w^{(0)} w_\eta^{(0)}]\,\mathrm{d}\eta \right\} - \tfrac{1}{2}\ln r \right]. \tag{2.54}$$

This expression is simplified by virtue of L'Hopital's rule to become

$$A = \kappa \left\{ \tfrac{1}{2} \lim_{r\to\infty} \left(\int_0^r \eta[v^{(0)}]^2\,\mathrm{d}\eta - \ln r \right) + \tfrac{1}{4} - \int_0^\infty \eta[w^{(0)}]^2\,\mathrm{d}\eta \right\}. \tag{2.55}$$

The form for the first-order velocity just given is equal to that derived by Widnall *et al.* (1971), Moore & Saffman (1972) and Callegari & Ting (1978).

For later use, we need the θ-dependence of the first-order velocities. Introducing (2.46) into (2.41), we get

$$u^{(1)} = \hat{u}^{(1)}(r,s,t)\sin\varphi, \tag{2.56}$$

$$v^{(1)} = \hat{v}^{(1)}(r,s,t)\cos\varphi. \tag{2.57}$$

The axial component of velocity is then found from (2.39) to be

$$w^{(1)} = \hat{w}_0^{(1)}(r,s,t) + \hat{w}^{(1)}(r,s,t)\cos\varphi, \tag{2.58}$$

with

$$\hat{w}^{(1)} = \frac{r\hat{u}^{(1)} w_r^{(0)}}{v^{(0)}} + \kappa r w^{(0)}. \tag{2.29}$$

Equation (2.56) is a result irrelevant to the neglect of the axisymmetric part of the stream function. It tells us that there is no net local radial convergence or divergence of flow that depends on the arclength s, which in turn implies that the non-uniform local stretching of the vortex line does not appear at this order. This may serve as some support to the hypothesis (2.49). The specification of the axisymmetric part $\hat{w}_0^{(1)}$ of the axial velocity is given at the end of the derivation.

Now we proceed to the calculation of the second-order perturbations. The second-order fields $(u^{(2)}, v^{(2)}, w^{(2)})$ can be shown to satisfy the following forms of the Euler equation (see the Appendix):

$$\frac{2w^{(0)}}{\sigma}\dot{\boldsymbol{X}}_\xi^{(0)}\cdot\boldsymbol{e}_r+u^{(1)}u_r^{(1)}+\frac{v^{(0)}u_\theta^{(2)}+v^{(1)}u_\theta^{(1)}-2v^{(0)}v^{(2)}-[v^{(1)}]^2}{r}$$
$$+w^{(0)}u_s^{(1)}+2\kappa w^{(0)}w^{(1)}\cos\varphi+\kappa^2 r[w^{(0)}]^2\cos^2\varphi=-p_r^{(2)}, \quad (2.60)$$

$$v_t^{(0)}+\frac{2w^{(0)}}{\sigma}\dot{\boldsymbol{X}}_\xi^{(0)}\cdot\boldsymbol{e}_\theta+u^{(1)}v_r^{(1)}+u^{(2)}v_r^{(0)}+\frac{v^{(0)}v_\theta^{(2)}+v^{(1)}v_\theta^{(1)}+v^{(0)}u^{(2)}+v^{(1)}u^{(1)}}{r}$$
$$+w^{(0)}v_s^{(1)}-2\kappa w^{(0)}w^{(1)}\sin\varphi-\kappa^2 r[w^{(0)}]^2\cos\varphi\sin\varphi=-\frac{1}{r}p_\theta^{(2)}, \quad (2.61)$$

$$w_t^{(0)}+v^{(0)}\dot{\boldsymbol{e}}_\theta\cdot\boldsymbol{t}+\frac{w^{(0)}}{\sigma}\dot{\boldsymbol{X}}_\xi^{(0)}\cdot\boldsymbol{t}+u^{(1)}w_r^{(1)}+u^{(2)}w_r^{(0)}+\frac{w_\theta^{(1)}v^{(1)}+w_\theta^{(2)}v^{(0)}}{r}+w^{(0)}w_s^{(1)}$$
$$-\kappa w^{(0)}u^{(1)}\cos\varphi+\kappa[w^{(1)}v^{(0)}+w^{(0)}v^{(1)}]\sin\varphi+\kappa^2 r w^{(0)}v^{(0)}\sin\varphi\cos\varphi=-p_s^{(1)}, \quad (2.62)$$

where σ represents the rate of local stretching:

$$\sigma=|\boldsymbol{X}_\xi|=\frac{\partial s}{\partial\xi}. \quad (2.63)$$

The equation of continuity is, to this order

$$[ru^{(2)}]_r+v_\theta^{(2)}+r\left[w_s^{(1)}+\frac{1}{\sigma}\dot{\boldsymbol{X}}_\xi^{(0)}\cdot\boldsymbol{t}\right]-\kappa r[v^{(1)}\cos\varphi]_\theta-\kappa\cos\varphi[r^2u^{(1)}]_r=0. \quad (2.64)$$

Recalling the behaviour of the first-order velocities (2.56)–(2.59), we observe from (2.60)–(2.64) that the second-order velocities $u^{(2)}$ and $v^{(2)}$ are divided into three parts; the axisymmetric part, the part proportional to $\cos\varphi$ or $\sin\varphi$ and that proportional to $\cos 2\varphi$ or $\sin 2\varphi$. The axisymmetric part has an influence on the evolution of the leading-order velocity profiles, through which the velocity of the vortex filament is indirectly affected. The third part is related to the fluid motion caused by the core deformation of elliptical shape and has nothing to do with the translational velocity of the vortex at this order. Since our primary interest is in the translational velocity, we deal exclusively with the velocity proportional to $\cos\varphi$ or $\sin\varphi$.

Retaining only the relevant terms, (2.60), (2.61) and (2.64) become simply

$$\frac{v^{(0)}u_\theta^{(2)}}{r}-\frac{2v^{(0)}v^{(2)}}{r}+\frac{2w^{(0)}}{\sigma}\dot{\boldsymbol{X}}_\xi^{(0)}\cdot\boldsymbol{e}_r+w^{(0)}u_s^{(1)}+2\kappa w^{(0)}\hat{w}_0^{(1)}\cos\varphi=-p_r^{(2)}, \quad (2.65)$$

$$\frac{v^{(0)}v_\theta^{(2)}}{r}+\frac{1}{r}[rv^{(0)}]_r u^{(2)}+\frac{2w^{(0)}}{\sigma}\dot{\boldsymbol{X}}_\xi^{(0)}\cdot\boldsymbol{e}_\theta+w^{(0)}v_s^{(1)}-2\kappa w^{(0)}\hat{w}_0^{(1)}\sin\varphi=-\frac{1}{r}p_\theta^{(2)}, \quad (2.66)$$

and

$$[ru^{(2)}]_r+v_\theta^{(2)}+rw_s^{(1)}=0. \quad (2.67)$$

In passing, we note that the terms in (2.65)–(2.67) correspond to those considered by Moore & Saffman (1972). The third terms on the left-hand sides of (2.65) and (2.66) come from the convection of the axial momentum along the tube axis and the apparent acceleration due to transfer of the coordinates to the moving frame. The fourth and fifth terms originate from the convection of the transverse and axial

momentum along the tube, respectively. Equation (2.67) means that the apparent distributions of sinks or sources appear in each two-dimensional cross-section of the tube on account of the variation of the axial mass flux along the tube.

Inserting (2.58) with (2.59) into (2.67), we find that the left-hand side of (2.67) vanishes by introducing a second-order stream function:

$$u^{(2)} = \frac{1}{r}\psi_\theta^{(2)}, \tag{2.68}$$

$$v^{(2)} = -\psi_r^{(2)} - r^2 w^{(0)}(\kappa_s \sin\varphi - \kappa\tau\cos\varphi) - \frac{r^2 w_r^{(0)}}{v^{(0)}}(\hat{u}_s^{(1)}\sin\varphi - \tau\hat{u}^{(1)}\cos\varphi). \tag{2.69}$$

We assume the following solution form for $\psi^{(2)}$:

$$\psi^{(2)} = \hat{\psi}_1^{(2)}\cos\varphi + \hat{\psi}_2^{(2)}\cos\varphi. \tag{2.70}$$

Then (2.65) and (2.66) are cast into the following forms:

$$\hat{\mathrm{L}}\hat{\psi}_1^{(2)} = \frac{2rw_r^{(0)}}{v^{(0)}\sigma}\boldsymbol{n}\cdot\dot{\boldsymbol{X}}_\xi^{(0)} + 2\kappa\tau r w^{(0)} + \frac{2\kappa r}{v^{(0)}}\frac{\partial}{\partial r}(w^{(0)}\hat{w}_0^{(1)}) + \frac{\tau}{v^{(0)}}[(3rw_r^{(0)} + r^2 w_{rr}^{(0)})\hat{u}^{(1)} - 3rw^{(0)}\hat{u}_r^{(1)} - r^2 w^{(0)}\hat{u}_{rr}^{(1)}], \tag{2.71}$$

$$\hat{\mathrm{L}}\hat{\psi}_2^{(2)} = \frac{2rw_r^{(0)}}{v^{(0)}\sigma}\boldsymbol{b}\cdot\dot{\boldsymbol{X}}_\xi^{(0)} - 2\kappa_s r w^{(0)} - \frac{1}{v^{(0)}}[(3rw_r^{(0)} + r^2 w_{rr}^{(0)})\hat{u}_s^{(1)} - 3rw^{(0)}\hat{u}_{rs}^{(1)} - r^2 w^{(0)}\hat{u}_{rrs}^{(1)}], \tag{2.72}$$

where the definition of $\hat{\mathrm{L}}$ is given by (2.48). The boundary conditions at the axis become

$$\hat{\psi}_1^{(2)} = \hat{\psi}_2^{(2)} = \frac{\partial\hat{\psi}_1^{(2)}}{\partial r} = \frac{\partial\hat{\psi}_2^{(2)}}{\partial r} = 0 \quad \text{at} \quad r = 0. \tag{2.73}$$

Equations (2.71) and (2.72) subject to the conditions (2.73) produce a solution in the form:

$$\begin{aligned}\hat{\psi}_1^{(2)} = {} & \frac{2\boldsymbol{n}\cdot\dot{\boldsymbol{X}}_\xi^{(0)}}{\sigma}v^{(0)}\int_0^r \frac{\mathrm{d}z}{z[v^{(0)}]^2}\left[\int_0^z \eta^2 w_\eta^{(0)}\,\mathrm{d}\eta\right] \\ & + 2\kappa\tau v^{(0)}\int_0^r \frac{\mathrm{d}z}{z[v^{(0)}]^2}\left[\int_0^z \eta^2 v^{(0)} w^{(0)}\,\mathrm{d}\eta\right] \\ & + 2\kappa v^{(0)}\int_0^r \frac{\mathrm{d}z}{z[v^{(0)}]^2}\left[\int_0^z \eta^2\frac{\partial}{\partial\eta}(w^{(0)}\hat{w}_0^{(1)})\,\mathrm{d}\eta\right] \\ & + \tau v^{(0)}\int_0^r \frac{\mathrm{d}z}{z[v^{(0)}]^2}\left[\int_0^z \{3\eta^2 w_\eta^{(0)} + \eta^3 w_{\eta\eta}^{(0)})\hat{u}^{(1)} - 3\eta^2 w^{(0)}\hat{u}_\eta^{(1)} - \eta^3 w^{(0)}\hat{u}_{\eta\eta}^{(1)}\}\,\mathrm{d}\eta\right],\end{aligned} \tag{2.74}$$

$$\begin{aligned}\hat{\psi}_2^{(2)} = {} & \frac{2\boldsymbol{b}\cdot\dot{\boldsymbol{X}}_\xi^{(0)}}{\sigma}v^{(0)}\int_0^r \frac{\mathrm{d}z}{z[v^{(0)}]^2}\left[\int_0^z \eta^2 w_\eta^{(0)}\,\mathrm{d}\eta\right] - 2\kappa_s v^{(0)}\int_0^r \frac{\mathrm{d}z}{z[v^{(0)}]^2}\left[\int_0^z \eta^2 v^{(0)} w^{(0)}\,\mathrm{d}\eta\right] \\ & - v^{(0)}\int_0^r \frac{\mathrm{d}z}{z[v^{(0)}]^2}\left[\int_0^z \{(3\eta^2 w_\eta^{(0)} + \eta^3 w_{\eta\eta}^{(0)})\hat{u}_s^{(1)} - 3\eta^2 w^{(0)}\hat{u}_{\eta s}^{(1)} - \eta^3 w^{(0)}\hat{u}_{\eta\eta s}^{(1)}\}\,\mathrm{d}\eta\right].\end{aligned} \tag{2.75}$$

Repeating the same matching procedure as for the first-order perturbations, we obtain

$$\dot{\boldsymbol{X}}^{(1)} = B_1(s,t)\,\boldsymbol{b} - B_2(s,t)\,\boldsymbol{n} + \boldsymbol{Q}^{(2)}, \tag{2.76}$$

where
$$B_1 = -\frac{2\boldsymbol{n}\cdot\dot{\boldsymbol{X}}_\xi^{(0)}}{\sigma}\int_0^\infty rw^{(0)}\,\mathrm{d}r + \kappa\tau\int_0^\infty r^2 v^{(0)}w^{(0)}\,\mathrm{d}r - 2\kappa\int_0^\infty rw^{(0)}\hat{w}_0^{(1)}\,\mathrm{d}r, \tag{2.77}$$

$$B_2 = -\frac{2\boldsymbol{b}\cdot\dot{\boldsymbol{X}}_\xi^{(0)}}{\sigma}\int_0^\infty rw^{(0)}\,\mathrm{d}r - \kappa_s\int_0^\infty r^2 v^{(0)}w^{(0)}\,\mathrm{d}r. \tag{2.78}$$

Bringing together the first-order velocity given by (2.53) and (2.55) and its second-order correction (2.76)–(2.78), we arrive at the final formula for the velocity of the vortex filament correct to the second order, which is written in terms of the dimensional variables as:

$$\begin{aligned}\dot{\boldsymbol{X}}(\xi,t) = {}& \frac{\kappa\Gamma}{4\pi}\Bigg[\ln\left(\frac{2L}{a}\right) - \tfrac{1}{2} + \lim_{r\to\tau}\left\{\frac{4\pi^2}{\Gamma^2}\int_0^r r[v^{(0)}]^2\,\mathrm{d}r - \ln\left(\frac{r}{a}\right)\right\} \\ & - \frac{8\pi^2}{\Gamma^2}\int_0^\infty r\{[w^{(0)}]^2 + 2\epsilon w^{(0)}\hat{w}_0^{(1)}\}\,\mathrm{d}r\Bigg]\boldsymbol{b} - \frac{4\pi}{\Gamma}\left[\int_0^\infty rw^{(0)}\,\mathrm{d}t\right]\boldsymbol{t}\times\frac{1}{\sigma}\dot{\boldsymbol{X}}_\xi^{(0)} \\ & - \frac{2\pi}{\Gamma}\left[\int_0^\infty r^2 v^{(0)}w^{(0)}\,\mathrm{d}r\right]\boldsymbol{t}\times\frac{\partial}{\partial s}(\kappa\boldsymbol{b}) + \boldsymbol{Q}.\end{aligned} \tag{2.79}$$

It was shown by Callegari & Ting (1978) that the axisymmetric parts of (2.61) and (2.62) determine the evolution of the leading-order velocities to be

$$w^{(0)}(r,t) = w^{(0)}(\alpha,0)\,l(0)/l(t), \tag{2.80}$$

$$\zeta^{(0)}(r,t) = \zeta^{(0)}(\alpha,0)\,l(t)/l(0): \tag{2.81}$$

thus
$$v^{(0)}(r,t) = v^{(0)}(\alpha,0)\,(l(t)/l(0))^{\frac{1}{2}}, \tag{2.82}$$

where $\alpha = r[l(t)/l(0)]^{\frac{1}{2}}$ and $l(t)$ is the total length of the filament.

It remains to specify the behaviour of the first-order correction $\hat{w}_0^{(1)}$ to the axisymmetric part of the axial velocity. The conservation of mass in the tube averaged over the core cross-section requires

$$\frac{\partial\xi}{\partial s}\frac{\partial}{\partial t}\left(a^2\frac{\partial s}{\partial\xi}\right) + \frac{\partial}{\partial s}(\bar{w}a^2) = 0, \tag{2.83}$$

where $\bar{w}$ is the axial velocity averaged over the core cross-section:

$$\bar{w} = \frac{1}{\pi a^2}\int_0^{2\pi}\int_0^\infty rw(r,\theta,s,t)\,\mathrm{d}r\,\mathrm{d}\theta. \tag{2.84}$$

Introducing the axisymmetric part of w given by

$$w = w^{(0)}(r,t) + \epsilon\hat{w}_0^{(1)}(r,s,t), \tag{2.85}$$

and (2.49) into (2.83), we find that

$$\frac{1}{a^2}\frac{\partial a^2}{\partial t} + \frac{\partial}{\partial t}\ln\sigma + \epsilon\frac{\partial\overline{\hat{w}_0^{(1)}}}{\partial s} + \frac{2\epsilon^2\overline{w^{(0)}}}{a}\frac{\partial a^{(2)}}{\partial s} = 0, \tag{2.86}$$

where the definition of σ is given by (2.63). It is easy to show that the local rate of stretching σ changes according to

$$\frac{\partial}{\partial t}\ln\sigma = \frac{\partial\theta_{\parallel}}{\partial s} - \kappa\boldsymbol{n}\cdot\dot{\boldsymbol{X}}. \tag{2.87}$$

The conservation of volume imposes a constraint on the evolution of the uniform part $a(t)$ of the core radius:

$$a(t)^2 l(t) = \text{constant}. \tag{2.88}$$

With these forms, (2.86) becomes

$$\epsilon\overline{\frac{\partial\hat{w}_0^{(1)}}{\partial s}} = -\frac{\partial\theta_{\parallel}}{\partial s} + \kappa\boldsymbol{n}\cdot\dot{\boldsymbol{X}}^{(0)} + \frac{1}{l}\frac{\mathrm{d}l}{\mathrm{d}t}. \tag{2.89}$$

The dependence of the total arclength l and t is determined by

$$\frac{\mathrm{d}l}{\mathrm{d}t} = \oint\frac{\partial}{\partial t}(\ln\sigma)\,\mathrm{d}s = -\oint\kappa\boldsymbol{n}\cdot\dot{\boldsymbol{X}}\,\mathrm{d}s. \tag{2.90}$$

To fix the constant that arises as the result of integration of (2.89), we invoke the conservation of the longitudinal circulation, i.e. the circulation along the vorticity centroid. With (2.58) supplemented by (2.59), we see that the longitudinal circulation is given by

$$\oint w(0,s,t)\,\mathrm{d}s = w^{(0)}(0,t)\,l(t) + \epsilon\oint\hat{w}_0^{(1)}(0,s,t)\,\mathrm{d}s. \tag{2.91}$$

If we assume that initially $\hat{w}_0^{(1)}(0,s,0) = 0$, then the conservation of the circulation enforces the condition

$$\oint\hat{w}_0^{(1)}(0,s,t)\,\mathrm{d}s = 0, \tag{2.92}$$

where use has been made of (2.80).

We notice that the resulting equation coincides with that of Moore & Saffman (1972). They took advantage of the approach based on the balance of forces acting on the surface of the vortex tube. The only difference lies in that they replace the filament curve by the osculating circle to the vortex at each point to evaluate the outer velocity field through the Biot–Savart integral. On the other hand, we approximated the filament curve by cubic polynomials in s.

In this stage, we can illustrate analytically how the axial flow affects the dispersion relation for long waves on columnar vortices, which extends the first-order form provided by Widnall *et al.* (1971), Moore & Saffman (1972) and Leibovich *et al.* (1986) to the second order. Consider a columnar vortex with arbitrary, but axisymmetric, distributions of axial and azimuthal vorticity. We introduce different cylindrical coordinates (ρ,ϕ,z) fixed in a rest frame such that the z-axis coincides with the centroid of vorticity. The appropriate choice of the basic velocity profile $(0, V_0, W_0)$ is Burgers' vortex expressed by

$$W_0(\rho) = W_{\mathrm{m}}\exp\left(-\alpha_1\frac{\rho^2}{a^2}\right), \tag{2.93}$$

$$V_0(\rho) = \frac{\Gamma}{2\pi\rho}\left[1-\exp\left(-\alpha_2\frac{\rho^2}{a^2}\right)\right]. \tag{2.94}$$

The parameter values $W_m/V_m = 0.4$, $\alpha_1 = 0.54$, $\alpha_2 = 1.28$ and $\Gamma/(2\pi a V_m) = 1.37$, where V_m is the maximum swirl velocity, fit the experimental data of Maxworthy *et al.* (1985). Alternatively, we can adopt Rankine's vortex, which is considered to be a discontinuous limit of the profiles (2.93) and (2.94).

Suppose that the properly defined core boundary is slightly perturbed like

$$\rho = a + D\cos(kz + m\phi - \omega t), \tag{2.95}$$

where $m = \pm 1$ for bending waves, making the assumption that

$$D \ll a, \quad |k|a \ll 1. \tag{2.96}$$

Then it immediately follows that the centroid $\boldsymbol{X}'$ of the vorticity is deflected off the z-axis to become

$$\boldsymbol{X}' = [D\cos(kz - \omega t), -mD\sin(kz - \omega t), z]. \tag{2.97}$$

With this form, the integration of the Biot–Savart formula (2.7) can be performed over the entire length in the form of expansions in powers of D/ρ, giving, to first order,

$$\boldsymbol{v}_1 = \frac{\Gamma}{2\pi\rho}\boldsymbol{e}_\phi + \nabla\Phi, \tag{2.98}$$

where $\boldsymbol{e}_\phi$ is the unit azimuthal vector and

$$\Phi = \frac{m|k|\Phi D}{2\pi} K_1(|k|\rho)\sin(kz + m\phi - \omega t), \tag{2.99}$$

with K_1 the second-kind modified Bessel function of first order. The curvature κ_0 and τ_0 of the curve (2.97) are

$$\kappa_0 = Dk^2, \quad \tau_0 = -mk. \tag{2.100}$$

We have two candidates for the unit of the outer variable due to the existence of two parameters given by (2.100). Since (2.96) implies that $D|k| \ll 1$, the preferred lengthscale characterizing the outer region is $1/|k|$. Then (2.98) and (2.99), when rewritten in terms of the local comoving cylindrical coordinates (r, θ, s), tends in the inner limit $a \ll r \ll 1/|k|$ to

$$\begin{aligned}\boldsymbol{v}_1 = {} & \frac{\Gamma}{2\pi r}\boldsymbol{e}_\theta + \frac{\Gamma D k^2}{4\pi}\left[\ln\left(\frac{2}{|k|r}\right) - \gamma - \tfrac{1}{2}\right]\boldsymbol{b} \\ & + \frac{\Gamma D k^2}{4\pi}\cos\varphi\,\boldsymbol{e}_\theta - \frac{m\Gamma D|k|^3 r}{4\pi}[\gamma + \ln(\tfrac{1}{2}|k|r) - \tfrac{1}{2}]\cos\varphi\,\boldsymbol{t} + O[\Gamma D k^2 (kr)^2],\end{aligned} \tag{2.101}$$

where γ is Euler's constant. Note that this limit is not inconsistent with the limit $a \ll r \ll 1/\kappa$ of our previous analysis. Equation (2.101) imposes the following boundary conditions for $r \gg a$ on the inner solution:

$$u^{(1)} = \frac{\Gamma D k^2}{4\pi}\left[\ln\left(\frac{2}{|k|r}\right) - \gamma - \tfrac{1}{2}\right]\sin\varphi - \dot{\boldsymbol{X}}^{(0)}\cdot\boldsymbol{e}_r, \tag{2.102}$$

$$v^{(1)} = \frac{\Gamma D k^2}{4\pi}\left[\ln\left(\frac{2}{|k|r}\right) - \gamma + \tfrac{1}{2}\right]\cos\varphi - \dot{\boldsymbol{X}}^{(0)}\cdot\boldsymbol{e}_\theta, \tag{2.103}$$

$$u^{(2)} = v^{(2)} = 0. \tag{2.104}$$

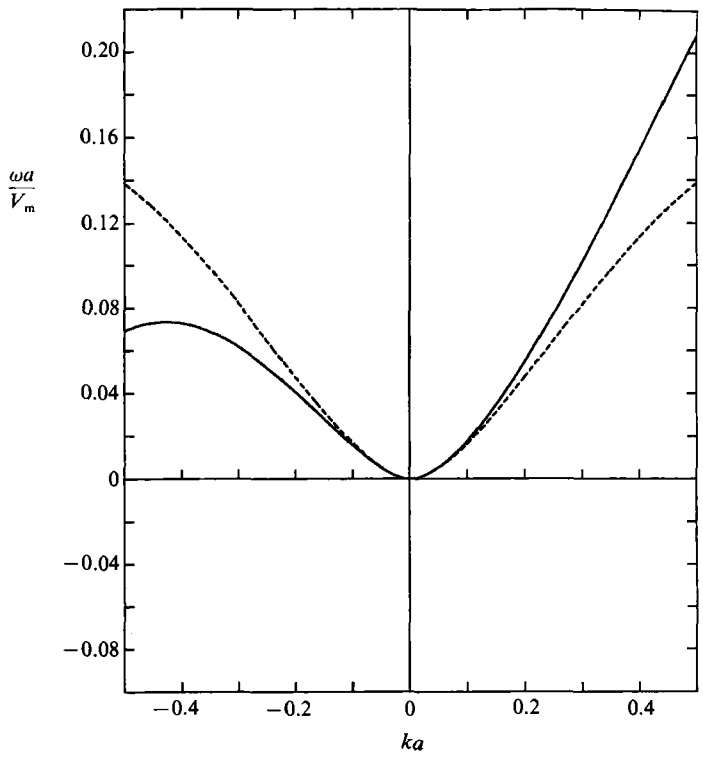

FIGURE 1. Asymptotic values of the dispersion relation for $m = -1$, for Burgers' vortex (2.93) and (2.94) with the parameters values given by Maxworthy *et al.* (1985). The solid line is the second-order formula (2.109). The dashed line is the first-order one.

The inner solution has already been provided by (2.41) with (2.50), and (2.68) and (2.69) with (2.70), (2.74) and (2.75). Thus the inner and outer solutions match if we take

$$\dot{X}(\xi,t) = \left\{\frac{\Gamma D k^2}{4\pi}C_1 - mDk^3\left[\left(\int_0^\infty rw^{(0)}\,\mathrm{d}r\right)C_1 + \frac{2\pi}{\Gamma}\left(\int_0^\infty r^2 v^{(0)}w^{(0)}\,\mathrm{d}r\right)\right]\right\}\boldsymbol{b}, \quad (2.105)$$

where

$$C_1 = \ln\left(\frac{2}{a|k|}\right) - \gamma + \lim_{r\to\infty}\left[\frac{4\pi^2}{\Gamma^2}\int_0^r r[v^{(0)}]^2\,\mathrm{d}r - \ln\left(\frac{r}{a}\right)\right] - \frac{8\pi^2}{\Gamma^2}\int_0^\infty r[w^{(0)}]^2\,\mathrm{d}r. \quad (2.106)$$

The vortex-line stretching is absent for this small-amplitude wave motion since $\dot{\boldsymbol{X}}^{(0)}\cdot\boldsymbol{n} = 0$. Comparison of (2.105) with the relation

$$\dot{X} = -m\omega D\boldsymbol{b} \quad (2.107)$$

gives rise to the dispersion relation valid to the second order:

$$\omega = -\frac{m\Gamma k^2}{4\pi}C_1 + k^3\left[\left(\int_0^\infty rw^{(0)}\,\mathrm{d}r\right)C_1 + \frac{2\pi}{\Gamma}\left(\int_0^\infty r^2 v^{(0)}w^{(0)}\,\mathrm{d}r\right)\right]. \quad (2.108)$$

This is an extension of the first-order formula. The same expression is given by Moore & Saffman (1972) for a helix of large pitch, permitting large lateral excursion. Fortunately, thanks to the restriction (2.96), our derivation is free from the ambiguity arising from the evaluation of the non-local induction.

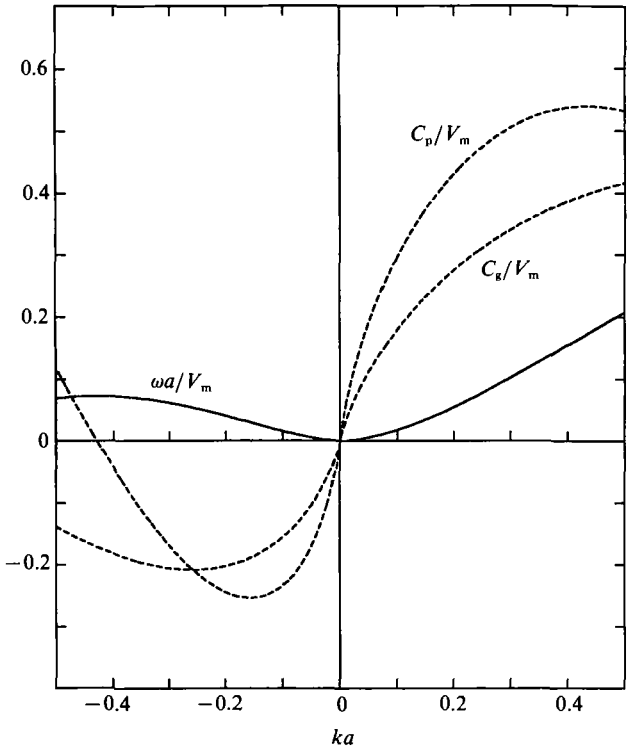

FIGURE 2. Asymptotic values of frequency, phase velocity C_p and group velocity C_g, valid to the second order, for the case of figure 1.

If the profile (2.93) and (2.94) is introduced, (2.108) takes the form

$$\omega = -\frac{m\Gamma k^2}{4\pi}\left[\ln\left(\frac{2}{a|k|}\right) - \tfrac{1}{2}\gamma + \tfrac{1}{2}\ln(\tfrac{1}{2}\alpha_2) - \frac{2\pi^2 W_m^2 a^2}{\Gamma^2\alpha_1}\right]$$
$$+ \tfrac{1}{2}W_m a^2 k^3\left\{\frac{1}{\alpha_1}\left[\ln\left(\frac{2}{a|k|}\right) - \tfrac{1}{2}\gamma + \tfrac{1}{2}\ln(\tfrac{1}{2}\alpha_2) - \frac{2\pi^2 W_m^2 a^2}{\Gamma^2\alpha_1}\right] + \frac{1}{\alpha_1} - \frac{1}{\alpha_1+\alpha_2}\right\}. \quad (2.109)$$

With the choice of the parameter values given by Maxworthy *et al.* (1985) and $m = -1$, we have plotted in figure 1 the normalized frequency as a function of the normalized wavenumber ka. For comparison, the values of the first-order formula are included. The departure from the first-order formula seems to agree, in the range of small wavenumbers, with that of the full numerical integration of the Howard–Gupta equation carried out by Leibovich *et al.* (1986), which is valid for all wavenumbers. Figure 2 shows the normalized frequency, phase and group velocities for the same case.

In order to advance the solution of (2.79) in time, we cannot help appealing to numerical computation. However, we expect that a simplified version may well capture some essential behaviour of the time evolution of a vortex filament. In the following section, we shall make an attempt to solve (2.79) directly.

3. Localized induction approximation

3.1. *Integrability*

In the previous section we have derived the Moore–Saffman equation (2.79) by a matching procedure. In order to make the axial-flow effect clearer, we simplify this equation by neglecting both the non-local induction $\boldsymbol{Q}$ and the variation of the cutoff parameter L/a along the vortex filament, as in the localized induction approximation. Under these assumptions we can replace $\dot{X}_\xi^{(0)}/\sigma$ in the second term of the right-hand side by the s-derivative of the first term. Then we find that the second and third terms have the same form proportional to $\boldsymbol{t}\times(\kappa\boldsymbol{b})_s$. If we use the arclength s instead of the marker variable ξ and renormalize the time, we have

$$\boldsymbol{X}_t = \kappa\boldsymbol{b} + \bar{W}(\tfrac{1}{2}\kappa^2\boldsymbol{t} + \kappa_s\boldsymbol{n} + \kappa\tau\boldsymbol{b}) = \boldsymbol{X}_s\times\boldsymbol{X}_{ss} + \bar{W}[\boldsymbol{X}_{sss} + \tfrac{3}{2}\boldsymbol{X}_{ss}\times(\boldsymbol{X}_s\times\boldsymbol{X}_{ss})], \tag{3.1}$$

$$\bar{W} = \frac{4\pi}{\Gamma}\int_0^\infty rw^{(0)}\,\mathrm{d}r + \frac{\dfrac{2\pi}{\Gamma}\displaystyle\int_0^\infty r^2v^{(0)}w^{(0)}\,\mathrm{d}r}{\dfrac{\Gamma}{4\pi}\left[\ln\left(\dfrac{2L}{a}\right)-\tfrac{1}{2}\right] + \lim_{r\to\infty}\left[\dfrac{\pi}{\Gamma}\displaystyle\int_0^r rv^{(0)^2}\,\mathrm{d}r - \dfrac{\Gamma}{4\pi}\ln\left(\dfrac{r}{a}\right)\right] - \dfrac{2\pi}{\Gamma}\displaystyle\int_0^\infty rw^{(0)^2}\,\mathrm{d}r}. \tag{3.2}$$

This new equation is a natural generalization of the LIE, which takes account of the axial-flow effect up to the second order. The parameter $\bar{W}$ represents the magnitude of the second-order effect.

Fortunately, this generalization preserves the most important property of the LIE, i.e. integrability. It is easy to see that the new equation (3.1) is reduced to the Hirota equation, by repeating Hasimoto's (1972) procedure which proved the equivalence between LIE and NLS (see also Lamb 1977). If we introduce a complex vector $\boldsymbol{N}$ in addition to the complex function ψ (1.4),

$$\psi = \kappa\exp\left(\mathrm{i}\int^s\tau\,\mathrm{d}s'\right), \quad \boldsymbol{N} = (\boldsymbol{n}+\mathrm{i}\boldsymbol{b})\exp\left(\mathrm{i}\int^s\tau\,\mathrm{d}s'\right), \tag{3.3}$$

the Serret–Frenet formulae

$$\boldsymbol{t}_s = \kappa\boldsymbol{n}, \quad \boldsymbol{n}_s = -\kappa\boldsymbol{t}+\tau\boldsymbol{b}, \quad \boldsymbol{b}_s = -\tau\boldsymbol{n} \tag{3.4}$$

are rewritten as

$$\boldsymbol{t}_s = \tfrac{1}{2}(\psi^*\boldsymbol{N}+\psi\boldsymbol{N}^*), \tag{3.5a}$$

$$\boldsymbol{N}_s = -\psi\boldsymbol{t}. \tag{3.5b}$$

The time evolution of the tangent vector $\boldsymbol{t}$ is given by differentiating (3.1) with respect to s:

$$\boldsymbol{t}_t = -\kappa\tau\boldsymbol{n} + \bar{W}[(\kappa_{ss}+\tfrac{1}{2}\kappa^3-\kappa\tau^2)\boldsymbol{n} + (2\kappa_s\tau+\kappa\tau_s)\boldsymbol{b}] = -\tfrac{1}{2}\gamma^*\boldsymbol{N} - \tfrac{1}{2}\gamma\boldsymbol{N}^*, \tag{3.6}$$

$$\gamma = -\mathrm{i}\psi_s - \bar{W}\psi_{ss} - \tfrac{1}{2}\bar{W}|\psi|^2\psi. \tag{3.7}$$

On the other hand, the time derivative of $\boldsymbol{N}$ can be expressed by

$$\boldsymbol{N}_t = \mathrm{i}R\boldsymbol{N} + \gamma\boldsymbol{t}, \tag{3.8}$$

where the identities $\boldsymbol{N}\cdot\boldsymbol{N} = 0$, $\boldsymbol{N}\cdot\boldsymbol{N}^* = 2$ and $\boldsymbol{N}\cdot\boldsymbol{t} = 0$ are considered. The real function R is determined from the compatibility of differentiations with respect to the time and the arclength:

$$\boldsymbol{N}_{ts} = \boldsymbol{N}_{st}, \tag{3.9}$$

which leads to

$$R_s = \tfrac{1}{2}\mathrm{i}(\gamma\psi^* - \gamma^*\psi), \tag{3.10}$$

$$\psi_t + \gamma_s - \mathrm{i}R\psi = 0. \tag{3.11}$$

Integration of (3.10), using (3.7), gives

$$R = \tfrac{1}{2}|\psi|^2 + \tfrac{1}{2}\mathrm{i}\bar{W}(\psi\psi_s^* - \psi_s\psi^*). \tag{3.12}$$

Then we have the Hirota (1973) equation after substituting (3.7) and (3.12) into (3.11):

$$\mathrm{i}\psi_t + \psi_{ss} + \tfrac{1}{2}|\psi|^2\psi - \mathrm{i}\bar{W}(\psi_{sss} + \tfrac{3}{2}|\psi|^2\psi_s) = 0. \tag{3.13}$$

The Hirota equation is the integrable equation that reduces to the nonlinear Schrödinger equation in the limit $\bar{W} \to 0$ and to the modified KdV equation as $\bar{W} \to \infty$, respectively. So, our new equation is integrable. It is remarkable that the integrability of the nonlinear evolution equation obtained under the assumptions of localized induction is not lost, even if the higher-order correction terms are considered. It will also be noted that (3.1) includes the local stretching term proportional to $(\kappa^2)_\xi$:

$$\frac{\partial}{\partial t}\left(\frac{\partial s}{\partial \xi}\right) = -\bar{W}\frac{\partial}{\partial \xi}(\tfrac{1}{2}\kappa^2)$$

whose integration from ξ_1 to ξ_2,

$$\frac{\mathrm{d}}{\mathrm{d}t}\int_{\xi_1}^{\xi_2} \mathrm{d}s = -\tfrac{1}{2}\bar{W}\kappa^2\Big|_{\xi_1}^{\xi_2}$$

shows that there is no total stretch for a closed vortex filament and a vortex filament straight at infinity.

Since the Hirota equation belongs to the class of integrable equations that are reduced to a system of linear equations by the AKNS formalism, we can apply the technique of the 'soliton surface approach' (Sym 1982, 1984) to (3.1) directly. This approach gives an illuminating geometrical interpretation of the above equivalence relation. Hirota's method of bilinear form is also convenient for writing the N-soliton solution explicitly, and the bilinear form of (3.1) is presented by Miyazaki & Fukomoto (1988). Anyway, the new equation (3.1) can be solved exactly and several solutions of physical interests are shown in the following sections.

3.2. *N-soliton solution*

According to the 'soliton surface approach' of Sym, the N-soliton solution can be generated by applying the Darboux–Bäcklund transformation to a 'straight line vortex' $\boldsymbol{X} = -s\boldsymbol{e}_z$, $\psi = 0$, successively. The Darboux–Bäcklund transformations (Levi, Ragnisco & Sym 1984) for the AKNS class of nonlinear integrable equations give the inter-relation between two solutions at four levels, i.e. first at the level of the scattering data, secondly at the level of the Jost solution, thirdly at the level of the potential ψ and lastly at the level of the soliton surface (vortex filament) $\boldsymbol{r}(\boldsymbol{X})$. They add one more bound state to the scattering data and generate a solution with one more soliton (soliton excitation). Thus the N-soliton solution is obtained by purely algebraic means. The actual calculation parallels that of the N-soliton solution of the LIE (Levi *et al.* 1983; Sym 1984, 1985), and we have only to replace the dispersion relation for each bound state in the case of the LIE by

$$\omega(\zeta_j) = -2\zeta_j^2 + 4\bar{W}\zeta_j^3, \tag{3.14}$$

where ζ_j is a discrete spectrum. The explicit form of the 1-soliton solution is given in Cartesian coordinates (x, y, z) by

$$\boldsymbol{X} = X\boldsymbol{e}_x + Y\boldsymbol{e}_y + Z\boldsymbol{e}_z$$

with
$$X+\mathrm{i}Y=\frac{q_1}{p_1^2+q_1^2}\operatorname{sech}\left(2q_1\{s-4[p_1-\bar{W}(q_1^2-3p_1^2)]t\}+c_1\right)$$
$$\times\exp\left(\mathrm{i}\{2p_1 s-4[p_1^2-q_1^2+2\bar{W}p_1(p_1^2-3q_1^2)]t-\phi_1\}\right), \quad (3.15)$$

$$Z=s-\frac{2q_1}{p_1^2+q_1^2}\tanh\left(2q_1\{s-4[p_1-\bar{W}(q_1^2-3p_1^2)]t\}+c_1\right), \quad (3.16)$$

where
$$\zeta_1=p_1+\mathrm{i}q_1 \quad (3.17)$$

and c_1 and ϕ_1 are arbitrary constants. This expression is identical to that of the Hasimoto soliton except for the modified dispersion relation (3.14).

This solution reminds us of two results concerning the experimental observations (Maxworthy *et al.* 1983, 1985). First, the soliton distortion shape is not affected at all by the existence of the axial flow inside the vortex core. Secondly, the envelope and phase velocities are modified as

$$4p_1\to 4[p_1-\bar{W}(q_1^2-3p_1^2)], \quad (3.18a)$$

$$\frac{2}{p_1}(p_1^2-q_1^2)\to\frac{2}{p_1}[p_1^2-q_1^2+2\bar{W}p_1(p_1^2-3q_1^2)]. \quad (3.18b)$$

Although we have not made quantitative comparisons, it may be noted that these results are consistent with the experimental results, at least qualitatively. The task of writing the N-soliton solution explicitly for $N\geqslant 2$ is rather tedious (see Miyazaki & Fukumoto 1988 and Fukumoto & Miyazaki 1986 for the explicit N-soliton solution in the bilinear form), so we content ourselves with giving the 2-soliton solution, which is sufficient to grasp the features of soliton interaction. Its expression is identical to that of the LIE obtained by Levi *et al.* (1983) and Sym (1984), if the dispersion relation is replaced by (3.14):

$$\begin{aligned}X_2+\mathrm{i}Y_2=&-\frac{\operatorname{Im}\zeta_1}{|\zeta_1|^2}\operatorname{sech}\eta_1\,\mathrm{e}^{\mathrm{i}\xi_1}-\frac{\operatorname{Im}\zeta_2}{|\zeta_2|^2}\frac{1}{T}\{[(\tfrac{1}{2}|\Delta|^2+\operatorname{Re}\Delta)\cosh\eta_2\\&+\tfrac{1}{2}|\Delta|^2\tanh\eta_1\sinh\eta_2-\mathrm{i}\operatorname{Im}\Delta\sinh\eta_2]\,\mathrm{e}^{\mathrm{i}\xi_1}\\&+[(1+\operatorname{Re}\Delta)\cosh\eta_1+\tfrac{1}{4}|\Delta|^2\operatorname{sech}\eta_1+\mathrm{i}\operatorname{Im}\Delta\sinh\eta_1]\,\mathrm{e}^{\mathrm{i}\xi_2}\\&+\tfrac{1}{4}|\Delta|^2\operatorname{sech}\eta_1\,\mathrm{e}^{\mathrm{i}(2\varphi_1-\varphi_2)}\},\end{aligned} \quad (3.19)$$

$$\begin{aligned}Z_2=&-s+\frac{\operatorname{Im}\zeta_1}{|\zeta_1|^2}\tanh\eta_1+\frac{\operatorname{Im}\zeta_2}{|\zeta_2|^2}\frac{1}{T}\{(\operatorname{Re}\Delta+\tfrac{1}{2}|\Delta|^2)\sinh\eta_1\cosh\eta_2\\&+(1+\operatorname{Re}\Delta+\tfrac{1}{2}|\Delta|^2)\sinh\eta_2\cosh\eta_1-\tfrac{1}{2}|\Delta|^2[\operatorname{sech}\eta_1\sinh\eta_2-\tanh\eta_1\cos(\xi_1-\xi_2)]\\&+\operatorname{Im}\Delta\sin(\xi_2-\xi_1)\},\end{aligned} \quad (3.20)$$

with
$$T=\cosh\eta_1\cosh\eta_2+(\operatorname{Re}\Delta+\tfrac{1}{2}|\Delta|^2)[\cos(\xi_1-\xi_2)+\cosh(\eta_1+\eta_2)]. \quad (3.21)$$

Here ζ_i ($i=1,2$) are the complex soliton parameters with positive imaginary parts and

$$\eta_i=2(\operatorname{Im}\zeta_i)s-2\operatorname{Im}[\omega(\zeta_i)]t+\eta_i^0, \quad (3.22)$$

$$\xi_i=2(\operatorname{Re}\zeta_i)s-2\operatorname{Re}[\omega(\zeta_i)]t+\xi_i^0, \quad (3.23)$$

$$\Delta=\frac{\zeta_2^*(\zeta_1^*-\zeta_1)}{\zeta_1^*(\zeta_1-\zeta_2^*)} \quad (3.24)$$

with η_i^0, ξ_i^0 being real constants.

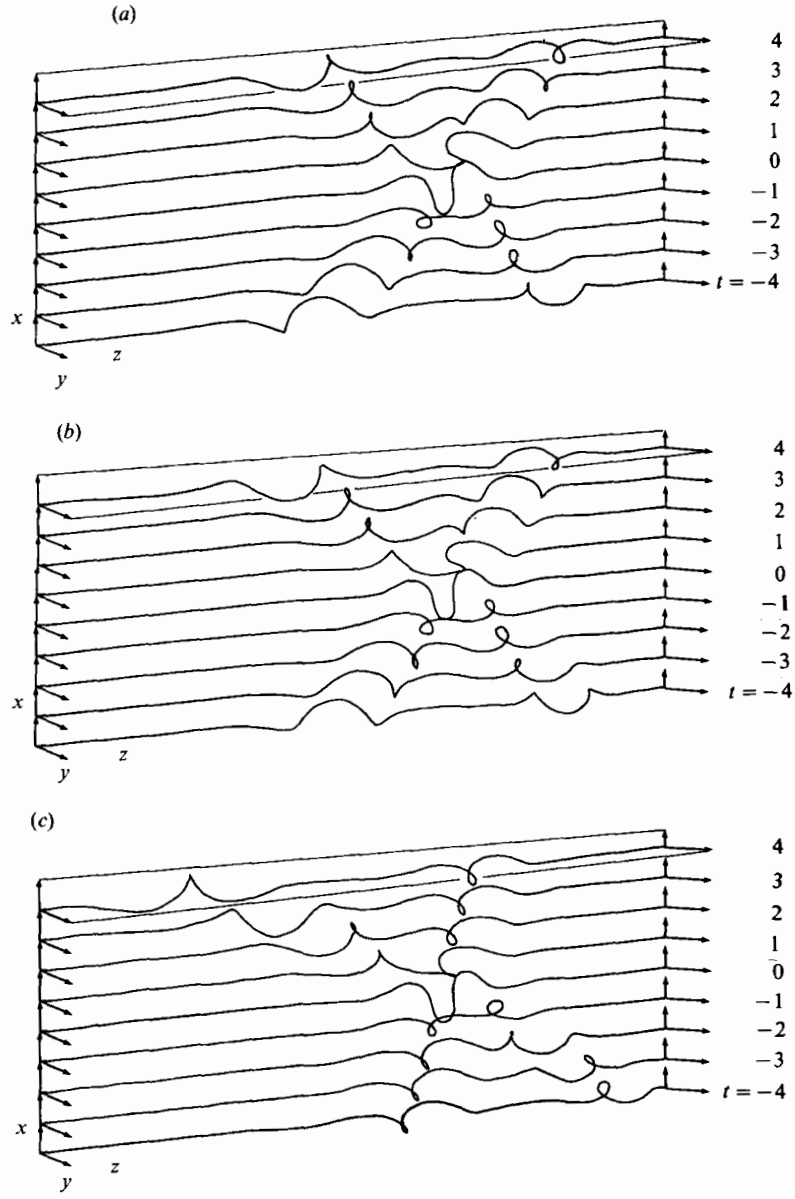

FIGURE 3. Perspective views of a head-on collision sequence between two solitons ($\zeta_{1,2} = \pm 0.5 + 0.25i$) for three values of $\bar{W}$: (*a*) $\bar{W} = 0$; (*b*) -0.1; (*c*) -0.5. Time increases upwards from -4 to 4.

We show perspective views of the two-soliton interaction ($\zeta_{1,2} = \pm 0.5 + 0.25i$) in figure 3(*a–c*). for $\bar{W} = 0$, -0.1 and -0.5, respectively. We can see from this figure that the phase shift during the collision of two solitons does not increase much even if the value of $|\bar{W}|$ is increased. Thus, we cannot explain the large phase advance observed in the experiment (Maxworthy *et al.* 1983) simply by considering the axial-flow effect under the localized induction approximation. This failure suggests that some dynamical factors neglected in the derivation of (3.1), such as the variation of the cutoff parameter along the vortex filament and the non-local induction, may

play an essential role in the multi-soliton interaction. Our next problem will be to take them into account.

Though our new approximate equation (3.1) does not always provide a good description of the quantitative findings of the laboratory experiments, it has the useful property of 'integrability' and we can obtain, besides the N-soliton solution, several exact solutions which show qualitatively new behaviour of the vortex filament with axial flow.

3.3. *Other particular solutions*

It is possible to find solutions of (3.1) that represent vortex distortions travelling and rotating steadily without change of form. Kida (1981) worked out such solutions of the LIE. Following his analysis, we assume that the vortex filament translates along the z-axis with constant velocity V and rotates around the z-axis with constant angular velocity Ω. Moreover, a steady slipping motion of the constant speed C is allowed:

$$\boldsymbol{X}_t = -C\boldsymbol{t} + \Omega \boldsymbol{e}_z \times \boldsymbol{X} + V\boldsymbol{e}_z. \tag{3.25}$$

This equation is integrated to give

$$\boldsymbol{X} = \rho(\xi)\,\boldsymbol{e}_\rho(\xi, t) + (z(\xi) + Vt)\,\boldsymbol{e}_z, \tag{3.26}$$

$$\xi = s - Ct, \tag{3.27}$$

where we employ a fixed cylindrical coordinate system (ρ, ϕ, z) and $\boldsymbol{e}_\rho$ is a unit vector in the radial direction defined by

$$\boldsymbol{e}_\rho = \cos(\phi(\xi) + \Omega t)\,\boldsymbol{e}_x + \sin(\phi(\xi) + \Omega t)\,\boldsymbol{e}_y. \tag{3.28}$$

we have, from (3.1) and (3.25) with (3.26),

$$-C\boldsymbol{t} + \Omega\rho\boldsymbol{e}_z \times \boldsymbol{e}_\rho + V\boldsymbol{e}_z = \kappa\boldsymbol{b} + \bar{W}(\tfrac{1}{2}\kappa^2\boldsymbol{t} + \kappa_s\boldsymbol{n} + \kappa\tau\boldsymbol{b}), \tag{3.29}$$

which determines the functions $\rho(\xi)$, $\phi(\xi)$ and $z(\xi)$ along with the constants V, Ω and C. Successive differentiations of (3.26) with respect to s give

$$\boldsymbol{t} = \rho_\xi \boldsymbol{e}_\rho + \rho\phi_\xi \boldsymbol{e}_z \times \boldsymbol{e}_\rho + z_\xi \boldsymbol{e}_z, \tag{3.30}$$

$$\kappa\boldsymbol{n} = (\rho_{\xi\xi} - \rho\phi_\xi^2)\,\boldsymbol{e}_\rho + (2\rho_\xi\phi_\xi + \rho\phi_{\xi\xi})\,\boldsymbol{e}_z \times \boldsymbol{e}_\rho + z_{\xi\xi}\boldsymbol{e}_z, \tag{3.31}$$

where the relation

$$\boldsymbol{e}_{\rho\xi} = \phi_\xi \boldsymbol{e}_z \times \boldsymbol{e}_\rho$$

is used, repeatedly. We see from (3.30) that

$$1 = \rho_\xi^2 + \rho^2 + \phi_\xi^2 + z_x^2, \tag{3.32}$$

and from (3.31) that

$$\kappa^2 = (\rho_{\xi\xi} - \rho\phi_\xi^2)^2 + (2\rho_\xi\phi_\xi + \rho\phi_{\xi\xi})^2 + z_{\xi\xi}^2. \tag{3.33}$$

The binormal vector and its s-derivative are written as

$$\begin{aligned}\kappa\boldsymbol{b} = \boldsymbol{t} \times \kappa\boldsymbol{n} &= (\rho\phi_\xi z_{\xi\xi} - 2\rho_\xi\phi_\xi z_\xi - \rho\phi_{\xi\xi} z_\xi)\,\boldsymbol{e}_\rho \\ &\quad + (\rho_{\xi\xi} z_\xi - \rho\phi_\xi^2 z_\xi - \rho_\xi z_{\xi\xi})\,\boldsymbol{e}_z \times \boldsymbol{e}_\rho + (2\rho_\xi^2\phi_\xi + \rho\rho_\xi\phi_{\xi\xi} - \rho\rho_{\xi\xi}\phi_\xi + \rho^2\phi_\xi^3)\,\boldsymbol{e}_z,\end{aligned} \tag{3.34}$$

and

$$\begin{aligned}(\kappa\boldsymbol{b})_s = &[(\rho\phi_\xi z_{\xi\xi} - 2\rho_\xi\phi_\xi z_\xi - \rho\phi_{\xi\xi} z_\xi)_\xi \\ &- \phi_\xi(\rho_{\xi\xi} z_\xi - \rho\phi_\xi^2 z_\xi - \rho_\xi z_{\xi\xi})]\,\boldsymbol{e}_\rho \\ &+ [\phi_\xi(\rho\phi_\xi z_{\xi\xi} - 2\rho_\xi\phi_\xi z_\xi - \rho\phi_{\xi\xi} z_\xi) \\ &+ (\rho_{\xi\xi} z_\xi - \rho\phi_\xi^2 z_\xi - \rho_\xi z_{\xi\xi})_\xi]\,\boldsymbol{e}_z \times \boldsymbol{e}_\rho \\ &+ (2\rho_\xi^2\phi_\xi + \rho\rho_\xi\phi_{\xi\xi} - \rho\rho_{\xi\xi}\phi_\xi + \rho^2\phi_\xi^3)_\xi\,\boldsymbol{e}_z.\end{aligned} \tag{3.35}$$

The inner product of (3.29) with $\boldsymbol{t}$ yields

$$-C+\Omega\rho^2\phi_\xi+Vz_\xi=\tfrac{1}{2}\bar{W}[(\rho_{\xi\xi}-\rho\phi_\xi^2)^2+(2\rho_\xi\phi_\xi+\rho\phi_{\xi\xi})^2+z_{\xi\xi}^2]. \tag{3.36}$$

Evaluating the vector product of (3.29) with $\boldsymbol{t}$,

$$\Omega\rho\boldsymbol{t}\times(\boldsymbol{e}_z\times\boldsymbol{e}_\rho)+V\boldsymbol{t}\times\boldsymbol{e}_z=-\kappa\boldsymbol{n}+\bar{W}(\kappa\boldsymbol{b})_s \tag{3.37}$$

we obtain, with the aid of (3.31) and (3.35), the following three equations corresponding to the $\boldsymbol{e}_z$, $\boldsymbol{e}_\rho$ and $\boldsymbol{e}_z\times\boldsymbol{e}_\rho$ components. Only two of them are independent, but we show them all for later use:

$$\Omega\rho\rho_\xi=-z_{\xi\xi}+\bar{W}(2\rho_\xi^2\phi_\xi+\rho\rho_\xi\phi_{\xi\xi}-\rho\rho_{\xi\xi}\phi_\xi+\rho^2\phi_\xi^3)_\xi, \tag{3.38}$$

$$-\Omega\rho z_\xi+V\rho\phi_\xi=-\rho_{\xi\xi}+\rho\phi_\xi^2+\bar{W}[(\rho\phi_\xi z_{\xi\xi}-2\rho_\xi\phi_\xi z_\xi-\rho\phi_{\xi\xi}z_\xi)_\xi -\phi_\xi(\rho_{\xi\xi}-\rho\phi_\xi^2 z_\xi-\rho_\xi z_{\xi\xi})], \tag{3.39}$$

$$-V\rho_\xi=-2\rho_\xi\phi_\xi-\rho\phi_{\xi\xi}+\bar{W}[\phi_\xi(\rho\phi_\xi z_{\xi\xi}-2\rho_\xi\phi_\xi z_\xi-\rho\phi_{\xi\xi}z_\xi) +(\rho_{\xi\xi}z_\xi-\rho\phi_\xi^2 z_\xi-\rho_\xi z_{\xi\xi})_\xi]. \tag{3.40}$$

Equations (3.32) and (3.36), coupled with two independent equations of (3.38)–(3.40), are solved to determine the vortex shape as well as its translation velocity V and rotation rate Ω. Although these equations seem fairly complicated in general, several simple particular solutions can be found.

(i) The first example is the 1-soliton solution already obtained in the previous subsection:

$$\rho(\xi)=\frac{q_1}{p_1^2+q_1^2}\operatorname{sech}(2q_1\xi), \tag{3.41}$$

$$\phi(\xi)=2p_1\xi, \tag{3.42}$$

$$z(\xi)=\xi-\frac{2q_1}{p_1^2+q_1^2}\tanh(2q_1\xi), \tag{3.43}$$

$$C=V=4[p_1-\bar{W}(q_1^2-3p_1^2)], \tag{3.44}$$

$$\Omega=4(p_1^2+q_1^2)(1+4\bar{W}p_1). \tag{3.45}$$

(ii) The second example is the helicoidal vortex filament which is given by assuming $\rho=$ constant. In this case, (3.32), (3.36), (3.38) and (3.39) become

$$1=\rho^2\phi_\xi^2+z_\xi^2, \tag{3.46}$$

$$-C+\Omega\rho^2\phi_\xi+Vz_\xi=\tfrac{1}{2}\bar{W}(\rho^2\phi_\xi^4+\rho^2\phi_{\xi\xi}^2+z_{\xi\xi}^2), \tag{3.47}$$

$$0=-z_{\xi\xi}+\bar{W}(\rho^2\phi_\xi^3)_\xi, \tag{3.48}$$

$$-\Omega\rho z_\xi+V\rho\phi_\xi=\rho\phi_\xi^2+\bar{W}[\rho(\phi_\xi z_{\xi\xi}-\phi_{\xi\xi}z_\xi)_\xi+\rho\phi_\xi^3 z_\xi]. \tag{3.49}$$

Integrating (3.48) and substituting it into (3.46), we notice that

$$\phi_\xi=p=\text{const.},\quad z_\xi=q=\text{const.}$$

Equations (3.47) and (3.49) give, using (3.46),

$$(\Omega-pC)\rho^2p+(V-qC)q=\tfrac{1}{2}\bar{W}\rho^2p^4,\quad -(\Omega-pC)q+(V-qC)p=p^2+\bar{W}p^3q.$$

Then we have,

$$\Omega-pC=-p^2q+\bar{W}(\tfrac{1}{2}\rho^2p^5-p^3q^2), \tag{3.50}$$

$$V-qC=\rho^2p^3+\tfrac{3}{2}\bar{W}\rho^2p^4q. \tag{3.51}$$

If the curvature κ and the torsion τ are used instead of p and q, we find, noting the relations $\kappa = \rho p^2$ and $\tau = pq$, that

$$\rho = \frac{\kappa}{\kappa^2+\tau^2}, \quad p = (\kappa^2+\tau^2)^{\frac{1}{2}}, \quad q = \frac{\tau}{(\kappa^2+\tau^2)^{\frac{1}{2}}}.$$

After substitution of (3.50) and (3.51) into (3.26), the helicoidal vortex filament of constant curvature κ and torsion τ is obtained:

$$\boldsymbol{X} = \frac{\kappa}{\kappa^2+\tau^2}(\cos\Theta\,\boldsymbol{e}_x + \sin\Theta\,\boldsymbol{e}_y) + Z\,\boldsymbol{e}_z \tag{3.52}$$

with
$$\Theta = \phi(\xi) + \Omega t = (\kappa^2+\tau^2)^{\frac{1}{2}}\{s - [\tau + \bar{W}(\tau^2 - \tfrac{1}{2}\kappa^2)]\,t\} + \phi_0, \tag{3.53}$$

$$Z = \frac{\tau}{(\kappa^2+\tau^2)^{\frac{1}{2}}}s + \frac{\kappa^2}{(\kappa^2+\tau^2)^{\frac{1}{2}}}(1 + \tfrac{3}{2}\bar{W}\tau)\,t + z_0. \tag{3.54}$$

Here, the axial-flow effect appears only as correction terms in the translation velocity and the rotation rate. However, it will be shown in the following subsection that the stability of a helicoidal vortex filament is profoundly affected by the presence of axial flow.

(iii) The third example is Euler's elastica, which is a plane curve of nul-torsion. Assuming $\phi = 0$ in (3.32), (3.36), (3,38) and (3.40), we have

$$1 = \rho_\xi^2 + z_\xi^2, \tag{3.55}$$

$$-C + Vz_\xi = \tfrac{1}{2}\bar{W}(\rho_{\xi\xi}^2 + z_{\xi\xi}^2), \tag{3.56}$$

$$\Omega\rho\rho_\xi = -z_{\xi\xi}, \tag{3.57}$$

$$-V\rho_\xi = \bar{W}(\rho_{\xi\xi}z_\xi - \rho_\xi z_{\xi\xi})_\xi. \tag{3.58}$$

Integration of (3.57) with respect to ξ yields

$$z_\xi = -\tfrac{1}{2}\Omega\rho^2 + 2k^2 - 1, \tag{3.59}$$

where k is a constant. After substituting it into (3.55), we have

$$\rho_\xi^2 + (\tfrac{1}{2}\Omega\rho^2 - 2k^2 + 1)^2 = 1, \tag{3.60}$$

which admits a solution expressed in terms of the Jacobian elliptic function:

$$\rho = 2\Omega^{-\frac{1}{2}}k\,\mathrm{cn}\,(\Omega^{\frac{1}{2}}\xi\,|\,k). \tag{3.61}$$

A dn-type solution is also possible, but it is unacceptable as a vortex filament for its represents a crossing curve in the plane. Integrating (3.59) with (3.61), we find that

$$z = \xi - 2\Omega^{-\frac{1}{2}}E(\Omega^{\frac{1}{2}}\xi\,|\,k) + z_0, \tag{3.62}$$

where
$$E(\zeta\,|\,k) = \int_0^\zeta \mathrm{d}n^2(\zeta'\,|\,k)\,\mathrm{d}\zeta'. \tag{3.63}$$

The remaining equations (3.56) and (3.58) determine the slip speed C and the translation velocity V, respectively:

$$C = \bar{W}\Omega(1 - 2k^2), \tag{3.64}$$

$$V = -\bar{W}\Omega. \tag{3.65}$$

Thus we obtain Euler's elastica:

$$\boldsymbol{X} = 2\Omega^{-\frac{1}{2}} k \,\mathrm{cn}\,(\Omega^{\frac{1}{2}}[s+\bar{W}\Omega(2k^2-1)\,t]\,|\,k) \times (\cos\Omega t\,\boldsymbol{e}_x + \sin\Omega t\,\boldsymbol{e}_y)$$
$$+\{s-2\bar{W}\Omega(1-k^2)\,t-2\Omega^{-\frac{1}{2}}E(\Omega^{\frac{1}{2}}[s+\bar{W}\Omega(2k^2-1)\,t]\,|\,k)+z_0\}\,\boldsymbol{e}_z. \quad (3.66)$$

It will be noted that the vortex filament only rotates without translation if $\bar{W}=0$ (LIE), whereas it must translate with the velocity $-\bar{W}\Omega$ if axial flow is present.

All these solutions happen to provide curves of constant torsion, whose shapes are not affected at all by the axial-flow effect. This remarkable fact can be seen clearly, if we substitute $\psi = \kappa \exp[\mathrm{i}(\tau_0 s-\omega_0 t)]$ into the Hirota equation (3.13):

$$(\omega_0-\tau_0^2-\bar{W}\tau_0^3)\,\kappa+(1+3\bar{W}\tau_0)\,(\kappa_{ss}+\tfrac{1}{2}\kappa^3)=0, \quad (3.67)$$

$$\kappa_t+(2\tau_0+3\bar{W}\tau_0^2)\,\kappa_s-\bar{W}(\kappa_{sss}+\tfrac{3}{2}\kappa^2\kappa_s)=0. \quad (3.68)$$

These equations can be simplified, assuming $1+3\bar{W}\tau_0 \neq 0$, to

$$\frac{\omega_0-\tau_0^2-\bar{W}\tau_0^3}{1+3\bar{W}\tau_0}\kappa+\kappa_{ss}+\tfrac{1}{2}\kappa^3=0, \quad (3.69)$$

$$\kappa_t+\frac{2\tau_0+\bar{W}\omega_0+8\bar{W}\tau_0^2(1+\bar{W}\tau_0)}{1+3\bar{W}\tau_0}\kappa_s=0. \quad (3.70)$$

Finally, we have

$$(\omega_0'-\tau_0^2)\,\kappa+\kappa_{\xi\xi}+\tfrac{1}{2}\kappa^3=0 \quad (3.71)$$

with

$$\xi = s-C't \quad (3.72)$$

and

$$C' = \frac{2\tau_0+\bar{W}\omega_0+8\bar{W}\tau_0^2(1+\bar{W}\tau_0)}{1+3\bar{W}\tau_0}, \quad (3.73)$$

$$\omega_0' = \tau_0^2+\frac{\omega_0-\tau_0^2(1+\bar{W}\tau_0)}{1+3\bar{W}\tau_0}. \quad (3.74)$$

We can see that the axial-flow effect is absorbed in the coefficients C' and ω_0', causing modification of the translation velocity and the rotation rate without changing the shape of distortion.

The case $1+3\bar{W}\tau_0=0$ is rather special, where the curvature κ obeys the modified KdV equation:

$$\kappa_t+\tau_0\kappa_s+\frac{1}{3\tau_0}(\kappa_{sss}+\tfrac{3}{2}\kappa^2\kappa_s)=0. \quad (3.75)$$

Since the modified KdV equation admits the N-soliton solution, we have the N-soliton solution of constant torsion $\tau_0=-1/(3\bar{W})$ as a special class of the solution obtained in §3.2. It is shown in the following subsection that the vortex with this particular torsion plays a key role in the stability analysis of a helicoidal vortex filament.

3.4. *Linear stability of a helicoidal vortex filament*

It is of interest to study the stability of the particular solutions. In particular, the stability of a helicoidal vortex filament is important from a practical view point and many investigations have been made of a vortex without axial flow. In this

subsection, we elucidate the second-order axial-flow effect on the linear stability of a helicoidal vortex, on the basis of (3.1).

Substituting (1.4) into (3.1), we have the intrinsic equations that describe the time evolution of the curvature κ and the torsion τ:

$$\kappa_t + 2\kappa_s\tau + \kappa\tau_s - \bar{W}(\tfrac{3}{2}\kappa^2\kappa_s + \kappa_{sss} - 3\kappa_s\tau^2 - 3\kappa\tau\tau_s) = 0, \tag{3.76}$$

$$-\tau_t + \left(\frac{\kappa_{ss}}{\kappa}\right)_s - 2\tau\tau_s + \kappa\kappa_s + \bar{W}\left[3\kappa\kappa_s\tau + \tfrac{3}{2}\kappa^2\tau_s + 3\left(\frac{\kappa_{ss}\tau}{\kappa}\right)_s + 3\left(\frac{\kappa_s\tau_s}{\kappa}\right)_s + \tau_{sss} - 3\tau^2\tau_s\right] = 0. \tag{3.77}$$

If the steady solution $\kappa = \kappa_0$, $\tau = \tau_0$ is perturbed as $\kappa = \kappa_0 + a\cos(ks - \omega t)$, $\tau = \tau_0 + b\sin(ks - \omega t)$ and only linear terms are retained in (3.76) and (3.77), we can show that the perturbation obeys the following dispersion relation:

$$\omega = 2k\tau_0 + \bar{W}k(k^2 + 3\tau_0^2 - \tfrac{3}{2}\kappa_0^2) \pm |1 + 3\bar{W}\tau_0|\, k(k^2 - \kappa_0^2)^{\frac{1}{2}}. \tag{3.78}$$

When $\bar{W} = 0$ on the right-hand side, this reduces to the dispersion relation obtained by Betchov (1965) in the case without axial flow. He found that the helicoidal vortex is unstable to perturbations of wavelength longer than $2\pi/\kappa_0$. The modification due to the presence of the axial flow $\bar{W}$ occurs as follows. If $\bar{W}\tau_0 > 0$ or $\bar{W}\tau_0 < -\frac{2}{3}$, the amplification rate of the unstable mode increases. On the other hand, if $-\frac{2}{3} < \bar{W}\tau_0 < 0$, the amplification rate decreases. The most remarkable fact is that a helicoidal vortex with torsion $\tau_0 = -1/(3\bar{W})$ is neutrally stable to any small perturbations. Thus the axial flow in the vortex core seems to have a stabilizing effect for certain helicoidal vortices. In this connection, we would like to point out that Maxworthy *et al.* (1985) observed several helicoidal vortices whose torsion fulfilled the condition $\bar{W}\tau_0 < 0$, indicating a qualitative agreement with our prediction.

Following Betchov (1965), we may interpret this stabilizing mechanism with the help of the analogy between the intrinsic equations (3.76) and (3.77) and the fluid-dynamical equations governing the motion of a one-dimensional compressible fluid. If we retain only the nonlinear effects, discarding all the terms of higher derivatives, (3.76) and (3.77) are reduced to the form

$$\lambda_t + (T\lambda)_s - \tfrac{3}{2}\bar{W}\lambda\lambda_s = 0, \tag{3.79}$$

$$\lambda(T_t + TT_s) - \tfrac{1}{2}[(1 + 3\bar{W}\tau)^2\lambda^2]_s + \frac{3\bar{W}}{4\lambda}\lambda_s^2 T_s = 0, \tag{3.80}$$

where

$$\lambda = \kappa^2 \tag{3.81}$$

$$T = 2\tau(1 + \tfrac{3}{2}\bar{W}\tau). \tag{3.82}$$

Aside from the last terms, we can regard (3.79) and (3.80) as equations of one-dimensional gas dynamics, where λ and T correspond to the density and the velocity, respectively. The last terms represent only a slight modification of the convection velocity of λ and T. The term playing the role of the pressure is

$$p = -\tfrac{1}{2}(+1 + 3\bar{W}\tau)^2\lambda. \tag{3.83}$$

This implies that the pressure decreases as the density λ increases if $1 + 3\bar{W}\tau \neq 0$. In other words, the fluid is acted on by a pressure force directed towards the region with

larger density, which causes the instability. This destabilizing pressure effect should be weak, if the value of the torsion fluctuates slightly around $\tau_0 = -1/(3\bar{W})$.

However, some caveats should be emphasized in making predictions. These results pertain to a local model and the relevance of the new LIE to the full three-dimensional Euler equation or even to the Moore–Saffman equation remains unclear. In fact, the stability of a vortex filament is sometimes too delicate to be described by the local model. For example, the Crow instability (Crow 1970) of two anti-parallel vortex filaments is not found under the localized induction approximation, since this instability is caused, essentially, by non-local effects. In the next section, we evaluate the influence of non-local induction on the stability of a helicoidal vortex filament with a view to consolidating our prediction.

4. Influence of the entire filament on the stability of a helicoidal vortex filament

When we deal with the motion of a thin vortex filament whose lateral excursion is not small, it is reasonable to carry out the Biot–Savart integration. The question of the effect of non-local induction on the stability of a helicoidal vortex filament was first addressed by Levy & Forsdyke (1928) in this way. Unfortunately the Biot-Savart integral necessarily entails the logarithmic divergence for the induced velocity on the filament itself, thus requiring subtle treatment of the vortex core. Their inadequate treatment of the singularity misled them to erroneous conclusions in some respects. A quite reliable procedure, called the 'cutoff' method, was devised by Crow (1970) and was refined by Widnall *et al.* (1971) and Moore & Saffman (1972). Its heart is to remove the singularity by introducing a cutoff, chosen so as to establish the known local steady velocity field (Saffman 1970; Widnall *et al.* 1971). We should bear in mind that this method, when applied to a vortex filament with large centreline deformation, still remains *ad hoc*.

Resorting to it, Widnall (1972) conducted an elaborate calculation of the stability of a helicoidal vortex, and she found three kinds of instability mode, one of which corresponds to that predicted by the local-induction model, i.e., the long-wave instability mode. This study, however, considers only the first-order effect of curvature. At the first order, the axial-flow effect is equivalent to thickening of the vortex core and consequently it acts to decrease the amplification rate of the long-wave mode. In this section, we extend Widnall's approach to the second order and the influence of the axial current is clarified when non-local induction is taken into account.

4.1. *A cutoff method extended to second order*

Let us consider an isolated infinite vortex filament with constant curvature and constant torsion which winds around a cylinder surface with radius R. Choose the Cartesian coordinates (x, y, z) or the cylindrical coordinates (ρ, ϕ, z), both fixed in a rest frame, with the z-axis along the central axis of the cylinder. In these coordinate systems, the helicoidal filament rotates about the z-axis with angular velocity Ω and translates in the z-direction with velocity V_A without change of form. We introduce a parameter K so that the tangent of the angle β of the vortex centreline from the horizontal satisfies the relation $\tan\beta = (RK)^{-1}$. Thus the unperturbed filament $\boldsymbol{X}_0 = X_0, Y_0, Z_0)$ is given in the form:

$$X_0 = R\cos(K'\xi + \Omega t), \quad Y_0 = R\sin(K'\xi + \Omega t), \quad Z_0 = \xi\sigma_0^2 + V_A t, \tag{4.1}$$

where $\sigma_0 = 1/(1+K^2R^2)^{\frac{1}{2}}$ and $K' = K\sigma_0^2 = K/(1+K^2R^2)$. The pitch of helix is $2\pi/K$.

We subject this filament to small perturbations in both normal and binormal directions expressed by

$$\boldsymbol{n} = \begin{pmatrix} -\cos\phi \\ -\sin\phi \\ 0 \end{pmatrix}, \quad \boldsymbol{b} = \begin{pmatrix} \sigma_0 \sin\phi \\ -\sigma_0 \cos\phi \\ RK\sigma_0 \end{pmatrix}, \tag{4.2}$$

where $\phi = K'\xi + \Omega t$. The perturbed filament $\boldsymbol{X} = (X, Y, Z)$ is written, in column-vector notation, as

$$\boldsymbol{X} = \begin{pmatrix} R\cos\phi \\ R\sin\phi \\ \xi\sigma_0^2 + V_A t \end{pmatrix} + \tilde{\xi} e^{ik\xi} \begin{pmatrix} RK'\sin\phi \\ -RK'\cos\phi \\ R^2K^2\sigma_0^2 \end{pmatrix} + \tilde{\rho} e^{ik\xi} \begin{pmatrix} \cos\phi \\ \sin\phi \\ 0 \end{pmatrix}. \tag{4.3}$$

If we define $\dot{\boldsymbol{X}}_{\text{rel}}$ to be the velocity of the vortex filament looked at in the coordinate system which rotates about the z-axis with angular velocity Ω and simultaneously translates in the z-direction with velocity V_A, then we deduce from (4.3) that

$$\begin{aligned} \dot{\boldsymbol{X}}_{\text{rel}} &= \dot{\boldsymbol{X}} - \Omega \mathbf{e}_z \times \boldsymbol{X} - V_A \mathbf{e}_z \\ &= \dot{\tilde{\xi}} e^{ik\xi} \begin{pmatrix} RK'\sin\phi \\ -RK'\cos\phi \\ R^2K^2\sigma_0^2 \end{pmatrix} + \dot{\tilde{\rho}} e^{ik\xi} \begin{pmatrix} \cos\phi \\ \sin\phi \\ 0 \end{pmatrix}. \end{aligned} \tag{4.4}$$

Since we intend to perform the linear stability analysis, we set $\tilde{\xi}, \tilde{\rho} \propto e^{\alpha t}$. In this case the right-hand side of (4.4) becomes simply $\alpha(\boldsymbol{X} - \boldsymbol{X}_0)$.

The crucial step is to carry through the calculation of $\dot{\boldsymbol{X}}$, Ω and V_A in (4.4). The quantity $\dot{\boldsymbol{X}}$ is the self-induced velocity due to the entire perturbed filament. We exploit the Moore–Saffman equation with an appropriate cut-off introduced into the logarithmically divergent Biot–Savart line integral. Inspection of (2.79) convinces us that Widnall's formula gives way to the following one:

$$\begin{aligned} \dot{\boldsymbol{X}}(\xi, t) = \dot{\boldsymbol{X}}^{(0)}(\xi, t) &- \frac{4\pi}{\Gamma} \epsilon \left[\int_0^\infty r w^{(0)} \hat{w}_0^{(1)} \, \mathrm{d}t \right] \kappa \boldsymbol{b} - \frac{4\pi}{\Gamma} \left[\int_0^\infty r w^{(0)} \, \mathrm{d}r \right] \boldsymbol{t} \times \frac{1}{\sigma} \dot{\boldsymbol{X}}_\xi^{(0)} \\ &- \frac{2\pi}{\Gamma} \left[\int_0^\infty r v^{(0)} w^{(0)} \, \mathrm{d}y \right] \boldsymbol{t} \times (\kappa \boldsymbol{b})_s. \end{aligned} \tag{4.5}$$

Here $\boldsymbol{X}^{(0)}(\xi, t)$ is the induced velocity, valid to the first order, supplied by the following integral:

$$\dot{\boldsymbol{X}}^{(0)} = -\frac{\Gamma}{4\pi} \int_{[l_c]} \frac{(\boldsymbol{X} - \boldsymbol{X}') \times \mathrm{d}\boldsymbol{X}'}{|\boldsymbol{X} - \boldsymbol{X}'|^3}, \tag{4.6}$$

where

$$\ln(l_c) = \ln(\tfrac{1}{2}a) + \tfrac{1}{2} - A^{(1)}, \tag{4.7}$$

with

$$A^{(1)} = \lim_{r \to \infty} \left\{ \frac{4\pi^2}{\Gamma^2} \int_0^r r[v^{(0)}]^2 \, \mathrm{d}r - \ln\left(\frac{r}{a}\right) \right\} - \frac{8\pi^2}{\Gamma^2} \int_0^\infty r[w^{(0)}]^2 \, \mathrm{d}r, \tag{4.8}$$

and the symbol $[l_c]$ signifies that we cut the line integral off an arclength l_c on either side of the point ξ under consideration. The effect of the axial velocity is present in

the cutoff parameter also, as seen from (4.7) and (4.8). The second term on the right-hand side of (4.5) is the contribution coming from the change in the cutoff length l_c owing to the vortex-line stretching. We have taken advantage of the result that the logarithmic singularity necessarily appears like $-(\Gamma/4\pi)\ln(l_c)$ in accord with the LIE (1.4). It should be remembered that the time-advancement of the leading-order velocities $v^{(0)}$ and $w^{(0)}$ is described by (2.80)–(2.82) and that the development of $\hat{w}_0^{(1)}$ and the total length $l(t)$ is described by (2.89) and (2.90) under the constraint (2.92).

The success of the evaluation of the induced velocity (4.5) hinges on the accuracy of the integration occurring in $\dot{X}_\xi^{(0)}$. Differentiation of (4.6) with respect to ξ results in

$$\begin{aligned}\frac{\dot{X}_\xi^{(0)}}{(\Gamma/4\pi)} = &-\int_{[\delta]}\left\{\frac{X_\xi\times X'_{\xi'}}{|X-X'|^3}+(X-X')\times X'_{\xi'}\left(\frac{\partial}{\partial\xi}\frac{1}{|X-X'|^3}\right)\right\}\mathrm{d}\xi'\\ &-\frac{[X(\xi)-X(\xi-\delta)]\times X_\xi(\xi-\delta)}{|X(\xi)-X(\xi-\delta)|^3}\left(1-\frac{\partial\delta}{\partial\xi}\right)\\ &+\frac{[X(\xi)-X(\xi+\delta)]\times X_\xi(\xi+\delta)}{|X(\xi)-X(\xi+\delta)|^3}\left(1+\frac{\partial\delta}{\partial\xi}\right),\end{aligned}\tag{4.9}$$

where δ is the cutoff in terms of the parameter ξ provided, in our case, by

$$\ln\delta = \ln\left(\frac{a}{2\sigma_0}\right)-A^{(1)}+\tfrac{1}{2}-\tilde{\rho}K'^2R\,\mathrm{e}^{\mathrm{i}k\xi}/\sigma_0^2,\tag{4.10}$$

because of the relation

$$\sigma=\frac{\partial s}{\partial\xi}=\left|\frac{\partial X}{\partial\xi}\right|=\sigma_0(1+\tilde{\rho}K'^2R\,\mathrm{e}^{\mathrm{i}k\xi}/\sigma_0^2),\tag{4.11}$$

and the notation $X'=X(\xi',t)$ is understood. The second integrand of (4.9) includes terms proportional to $|X_0-X_{0'}|^{-7}$ when expended in the perturbation amplitudes $\tilde{\xi}$ and $\tilde{\rho}$, which brings about strongly singular behaviour. A way round this difficulty is to make use of partial integration to convert (4.9) into the form

$$\begin{aligned}\frac{\dot{X}_\xi}{(\Gamma/4\pi)} = &-\int_{[\delta]}\left\{\frac{X_\xi\times X'_{\xi'}}{|X-X'|^3}+\frac{(X-X')\times X'_{\xi'\xi'}}{|X-X'|^3}\right.\\ &\left.-\frac{3[(X-X')\cdot(X_\xi-X'_{\xi'})]\,[(X-X')\times X'_{\xi'}]}{|X-X'|^5}\right\}\mathrm{d}\xi'\\ &-\frac{\partial\delta}{\partial\xi}\left[\frac{1}{\delta}+O(\delta)\right]\frac{X_\xi\times X_{\xi\xi}}{|X_\xi|^3}.\end{aligned}\tag{4.12}$$

From (4.10), we get

$$\frac{1}{\delta}\frac{\partial\delta}{\partial\xi}=-\frac{\mathrm{i}k\tilde{\rho}K'^2R}{\sigma_0^2}\mathrm{e}^{\mathrm{i}k\xi}.\tag{4.13}$$

The procedure to obtain the second term of (4.5) is the following: since the dependence of $\hat{w}_0^{(1)}$ on r remains unknown, we have no choice but to think of it as

$$-\frac{4\pi}{\Gamma}\left[\int_0^\infty rw^{(0)}\,\mathrm{d}r\right]\overline{\epsilon\hat{w}_0^{(1)}}\kappa\boldsymbol{b}.\tag{4.14}$$

Integration of (2.89) yields

$$\overline{\epsilon\hat{w}_0^{(1)}} = -Q_{\parallel} + \int^{s} \kappa \boldsymbol{n}\cdot\dot{\boldsymbol{X}}^{(0)}\,\mathrm{d}s + \frac{s}{l}\frac{\mathrm{d}l}{\mathrm{d}t}. \tag{4.15}$$

The time-variation of the total arclength given by (2.90) is written, to the second order in curvature effect, as

$$\frac{\mathrm{d}l}{\mathrm{d}t} = -\int_{-\infty}^{\infty} \dot{\boldsymbol{X}}^{(0)}\cdot\boldsymbol{t}_{\xi}\,\mathrm{d}\xi. \tag{4.16}$$

For our configuration of the helicoidal filament, we have, after several manipulations,

$$\dot{\boldsymbol{X}}^{(0)}\cdot\boldsymbol{t}_{\xi} \propto \mathrm{e}^{\mathrm{i}k\xi}. \tag{4.17}$$

Hence it is a rational assumption that

$$l(t) = l(0) = \text{const.} \quad \text{for} \quad k \neq 0. \tag{4.18}$$

It is obvious that the helicoidal vortex is neutrally stable to perturbations with $k = 0$. Notice that the absence of vortex-line stretching is inherent in the linear stability analysis. For finite-amplitude perturbations, the vortex filament goes through significant line stretching, as a consequence of which its time evolution might be greatly different from the prediction of the linear analysis. The first term $Q_{\parallel} = \boldsymbol{t}\cdot\dot{\boldsymbol{X}}^{(0)}$ and the second integral are divided into two parts: the constant terms and those proportional to $\mathrm{e}^{\mathrm{i}k\xi}$. In view of the stipulation (2.92), we discard the constant terms, retaining only the latter ones. Thus we complete the prescription.

The calculation is carried out in much the same way as Widnall (1972). Without loss of generality, we may consider the specific point $\boldsymbol{X}(\xi, t)$ whose arclength parameter ξ fulfils the relation $K'\xi + \Omega t = 0$ at some instant t. It follows from (4.3) that some of the necessary formulae for position vectors are

$$\boldsymbol{X} = \begin{pmatrix} R \\ 0 \\ \xi\sigma_0^2 + V_{\mathrm{A}}\,t \end{pmatrix} + \tilde{\xi}\,\mathrm{e}^{\mathrm{i}k\xi}\begin{pmatrix} 0 \\ -RK' \\ R^2K^2\sigma_0^2 \end{pmatrix} + \tilde{\rho}\,\mathrm{e}^{\mathrm{i}k\xi}\begin{pmatrix} 1 \\ 0 \\ 0 \end{pmatrix}, \tag{4.19}$$

$$\boldsymbol{X}' = \begin{pmatrix} R\cos\bar{\phi} \\ R\sin\bar{\phi} \\ \xi'\sigma_0^2 + V_{\mathrm{A}}\,\mathrm{t} \end{pmatrix} + \tilde{\xi}\,\mathrm{e}^{\mathrm{i}k\xi'}\begin{pmatrix} RK'\sin\bar{\phi} \\ -RK'\cos\bar{\phi} \\ R^2K^2\sigma_0^2 \end{pmatrix} + \tilde{\rho}\,\mathrm{e}^{\mathrm{i}k\xi'}\begin{pmatrix} \cos\bar{\phi} \\ \sin\bar{\phi} \\ 0 \end{pmatrix}, \tag{4.20}$$

$$\boldsymbol{X}'_{\xi'} = \begin{pmatrix} -RK'\sin\bar{\phi} \\ RK'\cos\bar{\phi} \\ \sigma_0^2 \end{pmatrix} + \tilde{\xi}\,\mathrm{e}^{\mathrm{i}k\xi'}\begin{pmatrix} RK'^2\cos\bar{\phi} + \mathrm{i}kRK'\sin\bar{\phi} \\ RK'^2\sin\bar{\phi} - ikRK'\cos\bar{\phi} \\ \mathrm{i}kR^2K^2\sigma_0^2 \end{pmatrix}$$

$$+ \tilde{\rho}\,\mathrm{e}^{\mathrm{i}k\xi'}\begin{pmatrix} -K'\sin\bar{\phi} + \mathrm{i}k\cos\bar{\phi} \\ K'\cos\bar{\phi} + \mathrm{i}k\sin\bar{\phi} \\ 0 \end{pmatrix}, \tag{4.21}$$

where $\bar{\phi} = K'(\xi' - \xi)$.

The next step is to substitute these formulae into (4.5), (4.6) and (4.12), and to expand the resulting expressions in powers of $\tilde{\xi}$ and $\tilde{\rho}$ to first order. The explicit form of the induced velocity is not written out in full because the resulting expressions are

too lengthy. For convenience, we present the representations only of the angular velocity Ω and the translational velocity V_A of the unperturbed filament, including the second-order effect:

$$\Omega = \left(\frac{\Gamma}{4\pi} + W_1 K'\right)\sigma_0^2 \int_{-\infty}^{\infty} \frac{1-\cos\bar{\phi} - K'\bar{\xi}\sin\bar{\phi}}{[2R^2(1-\cos\bar{\phi}) + \sigma_0^4\bar{\xi}^2]^{\frac{3}{2}}}\,\mathrm{d}\bar{\xi} + W_2\sigma_0^5(-K^3 + \tfrac{1}{2}R^2K^5), \quad (4.22)$$

$$V_A = \frac{\Gamma R^2 K'}{4\pi}\int_{-\infty}^{\infty} \frac{1-\cos\bar{\phi}}{[2R^2(1-\cos\bar{\phi}) + \sigma_0^4\bar{\xi}^2]^{\frac{3}{2}}}\,\mathrm{d}\bar{\xi}$$

$$- W_1 R^2 K'^2 \int_{-\infty}^{\infty} \frac{1-\cos\bar{\phi} - K'\bar{\xi}\sin\bar{\phi}}{[2R^2(1-\cos\bar{\phi}) + \sigma_0^4\bar{\xi}^2]^{\frac{3}{2}}}\,\mathrm{d}\bar{\xi} + \tfrac{3}{2}W_2 R^2\sigma_0^5 K^5, \quad (4.23)$$

where $\bar{\phi} = K'\bar{\xi}$ and

$$W_1 = \int_0^{\infty} r w^{(0)}\,\mathrm{d}r, \quad W_2 = \frac{2\pi}{\Gamma}\left[\int_0^{\infty} r^2 v^{(0)} w^{(0)}\,\mathrm{d}r\right]. \quad (4.24)$$

The singular integrals that we encounter are treated in the same way as Widnall; the piece of length 2δ centred on ξ is subtracted off the integrand. The proper choice of δ is given by (4.10) but in most cases it is sufficient only to take

$$\ln\delta_0 = \ln\left(\frac{a}{2\sigma_0}\right) - A^{(1)} + \tfrac{1}{2}. \quad (4.25)$$

The small change of δ due to perturbation $\tilde{\rho}$ has no influence on $\dot{X}_\xi^{(0)}$ except for a small correction term

$$\frac{\Gamma}{4\pi}\frac{R^2K'^5}{\sigma_0^3}\tilde{\rho}\,\mathrm{e}^{\mathrm{i}k\xi}\boldsymbol{e}_\rho. \quad (4.26)$$

Now we have a vector equation for $\dot{\tilde{\xi}}$ and $\dot{\tilde{\rho}}$. Taking the scalar product of (4.4) with $\boldsymbol{b}$ and $\boldsymbol{n}$ at ξ and assuming that $\tilde{\xi}, \tilde{\rho} \propto \mathrm{e}^{\alpha t}$, we get a set of equations coupling $\tilde{\xi}$ and $\tilde{\rho}$. They constitute a linear eigenvalue problem for α.

We non-dimensionalize the result based upon the cylinder radius R and the characteristic velocity $\Gamma/(4\pi R)$. The dimensionless amplification rate $\bar{\alpha}$ is then defined as

$$\bar{\alpha} = \frac{\alpha}{\Gamma/(4\pi R^2)}, \quad (4.27)$$

and the parameters characterizing the axial velocity are

$$\bar{W}_1 = \frac{4\pi}{\Gamma R}W_1, \quad \bar{W}_2 = \frac{4\pi}{\Gamma R}W_2. \quad (4.28)$$

In general, the normalized amplification rate $\bar{\alpha}$ is a function of k, RK, a/R and $\bar{W}_1$ (or W_2). It is not difficult to confirm that $\bar{\alpha} = \bar{\alpha}\,(k;\, RK,\, \bar{W}_1,\, a/R)$ has the following symmetries:

$$\left.\begin{aligned} \bar{\alpha}(k; -Rk, \bar{W}_1, a/R) &= -\bar{\alpha}(k; RK, -\bar{W}_1, a/R), \\ \bar{\alpha}(-k; RK, \bar{W}_1, a/R) &= -\bar{\alpha}(k; RK, \bar{W}_1, a/R), \\ \bar{\alpha}(-k; -RK, \bar{W}_1, a/R) &= \bar{\alpha}(k; RK, -\bar{W}_1, a/R). \end{aligned}\right\} \quad (4.29)$$

We therefore restrict the range of the parameters to

$$k \geqslant 0 \quad \text{and} \quad K > 0. \tag{4.30}$$

In other words, we restrict our attention to right-handed helices or those of positive torsion K'.

4.2. *Results*

To facilitate the comparison with the first-order results, we take, as the basic velocity profiles, Rankine's vortex with a top-hat jet core. Its velocity profiles are

$$v^{(0)}(r) = \begin{cases} \dfrac{\Gamma}{2\pi a^2} r \\ \dfrac{\Gamma}{2\pi r} \end{cases}, \quad w^{(0)}(r) = \begin{cases} W = \text{const.} & \text{for} \quad 0 < r \leqslant a \\ 0 & \text{for} \quad r > a \end{cases}. \tag{4.31}$$

Introduction of (4.31) into (4.8) produces

$$A^{(1)} = \tfrac{1}{4} - \left(\frac{W}{V}\right)^2 \tag{4.32}$$

where $V = \Gamma/(2\pi a)$ is the maximum swirl velocity. The parameters $\overline{W}_1$ and $\overline{W}_2$ become

$$\overline{W}_1 = \frac{aW}{RV}, \quad \overline{W}_2 = \frac{aW}{2RV}. \tag{4.33}$$

The computation of $\bar{\alpha}$ is implemented for various pitch angles $\tan\beta = (RK)^{-1}$ and a/R with the velocity ratio W/V ranging from moderate negative values to moderate positive values. The numerical integration of the regularized Biot–Savart integral is done by making use of a standard fast-Fourier-transform subroutine. In an effort to confirm the correctness of our procedure, we have checked that the terms proportional to $-\ln a$ of the induction velocity do agree with the generalized localized induction equation (3.1), numerically as well as analytically.

In order to gain an insight into the general features of the effect of the axial flow, we first discuss the case of $\tan\beta = 1$ at some length. Figures 4(*a*) and 4(*b*) show the values of the amplification rate $\bar{\alpha}$ plotted against the normalized wavenumber k/K' for $a/R = 0.1$ and various velocity ratios ((*a*) for $W/V \leqslant 0$ and (*b*) $W/V \geqslant 0$). Figures 4(*c*) and 4(*d*) show the case of $a/R = 0.33$ for (*c*) $W/V \leqslant 0$ and (*d*) $W/V \geqslant 0$. The quantity k/K' has the simple meaning that it equals the number of waves in one period of a helicoid. When the axial flow is absent, the values obtained by Widnall (1972) are restored, which are represented by dashed lines. Corresponding to them is the long-wave instability mode.

We observe from figure 4(*a*) that the amplification rate of the long-wave mode monotonically decreases as W/V decreases from zero and that the long-wave mode disappears completely below some value of W/V a little less than -1. If we further decrease W/V, the short-wave instability mode comes out at smaller wavenumbers, whose growth rate decreases with W/V. Eventually the short-wave instability mode intrudes into the long-wave range, i.e. $k/K' \leqslant RK\sigma_0$, at some value of W/V a little less than -1.5. In contrast, in the case of $W/V \geqslant 0$ (figure 4*b*), the long-wave instability strengthens when W/V is slightly above zero. But further increase of W/V, in turn, reduces the amplification rate and the long-wave mode again subsides at

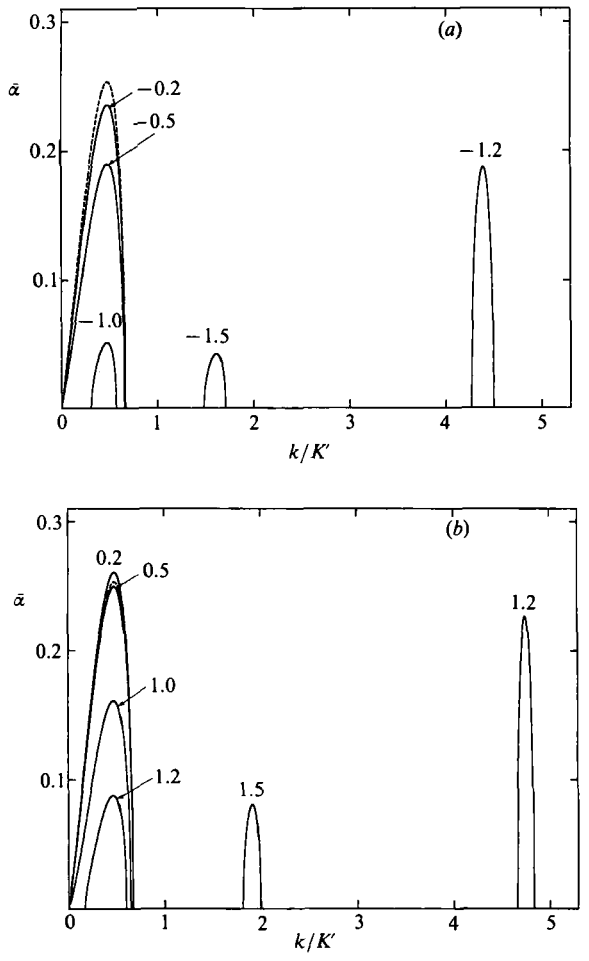

FIGURE 4(a, b). For caption see facing page.

moderate values of W/V. The magnitude of W/V at which the long-wave mode first vanishes is larger when $W/V > 0$. The later stage of the development of the short-wave mode, associated with the increment of W/V, is similar to the former case $W/V \leqslant 0$ except that here $|W/V|$ is larger. The long-wave mode reappears at some value of W/V. Turning to figure 4(c), we notice that thickening of the vortex core reduces the amplification rate of this mode and considerably promotes its stabilization. Indeed, for $a/R = 0.33$ and $W/V < 0$, the disappearance of the long-wave mode takes place at values of $|W/V|$ much smaller than those for the case of $a/R = 0.1$. With regard to the short-wave mode, the manner in which it approaches the long-wave regime at larger values of $|W/V|$ and the re-establishment of the long-wave mode occurs is similar to the case of $a/R = 0.1$ if the magnitude of W/V is appropriately shifted. Comparing figures 4(b) and 4(d), we find that the destabilizing effect of the small positive axial velocity is more prominent for the case of $a/R = 0.33$.

Let us compare these results with those of the local-induction model. The helicoidal vortices considered here have positive values of torsion $\tau = K'$. The local-induction equation predicts that for $\tau > 0$, the helicoidal vortex is stabilized only at

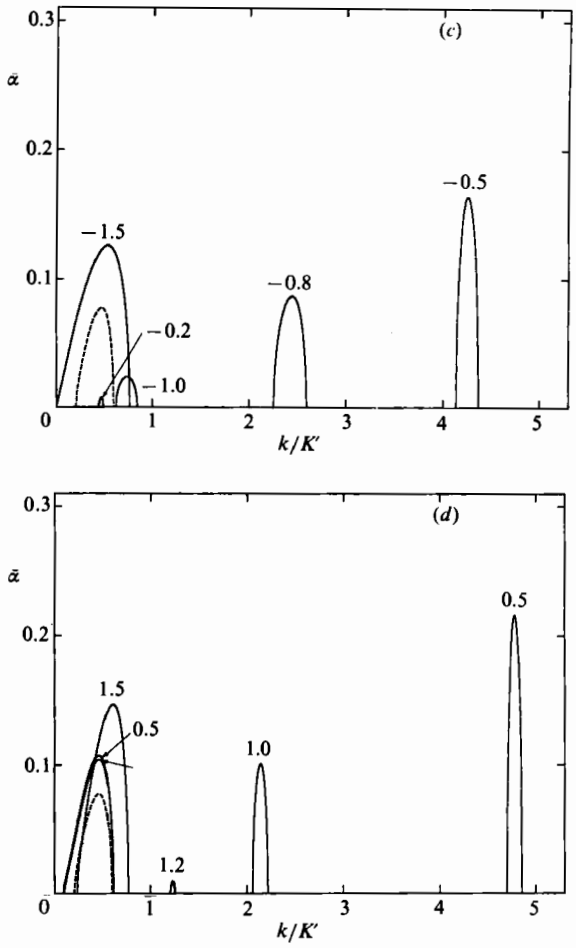

FIGURE 4. Non-dimensional amplification rate, for helices with the pitch angle $\tan\beta = 1$ and typical values of a/R (the ratio of vortex-core radius to cylinder radius), as a function of k/K' waves per cycle. The values of the ratio W/V of axial-to-swirl velocity are indicated on each curve. The dashed line is Widnall's (1972) result for $W/V = 0$. (*a*) $a/R = 0.1$, $W/V \leqslant 0$; (*b*) $a/R = 0.1$, $W/V \geqslant 0$; (*c*) $a/R = 0.33$, $W/V \leqslant 0$; (*d*) $a/R = 0.33$, $W/V \geqslant 0$.

the special value of W/V that is negative. In the cutoff model, there exists a range of W/V (< 0) for which the long-wave instability mode is absent. This band is not as wide and we may understand that the agreement is quite good between two models. The crucial difference lies in the case $W/V > 0$. In the local-induction approximation, the amplification rate monotonically increases with W/V. In the cut-off model, it increases for small W/V, a tendency is consistent with the former model, but it decreases for larger values of W/V and stabilization of the long-wave mode also occurs in a finite range of W/V. The source of the stabilization may be traced back to the dependence of the cut-off parameter on the velocity distribution as indicated by (4.7) and (4.8). the local-induction approximation disregards this point and it assumes merely that the parameter, dependent on the internal core structure, is a positive constant. This failure is discussed further in the next subsection.

The local model does not predict the short-wave instability mode. This is not the case with the cutoff model. Our method relies upon asymptotic expansions in powers

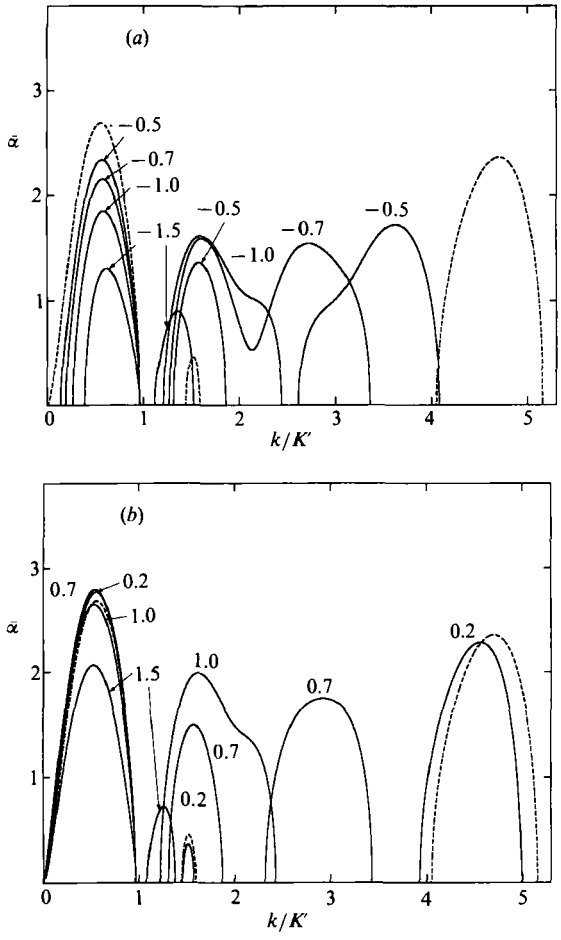

FIGURE 5. As figure 4 but with $\tan\beta = 0.3$. (a) $a/R = 0.33$, $W/V \leqslant 0$; (b) $a/R = 0.33$, $W/V \geqslant 0$.

of the small parameters $a\kappa(\kappa = RK'^2/\sigma_0^2)$ and ak. In effect, the instability of short wavelength of order a predicted by the cutoff approximation is spurious, which was exemplified by Moore & Saffman (1974). An analysis of the Euler equation for a vortex filament with no axial flow shows that, in the short-wavelength range, only bending modes with a more complex core structure are unstable (Widnall, Bliss & Tsai 1974; Moore & Saffman 1975; Tsai & Widnall 1976; Widnall & Tsai 1977; Saffman 1978). The short-wave mode which our cut-off model deduces may also be a result of an unjustified extrapolation.

There is another point that we must be cautious about. In view of the dispersion relation (2.108) and the full equation (4.5), the measure of the relative significance of the second-order terms to the first-order ones is given by $\overline{W}_1$ or $\overline{W}_2$. Hence our asymptotic expansions, upon which the cut-off method is based, rest on the smallness not only of κa and ka but also of $(W/V)\kappa a$ and $(W/V)ka$. The band of stability in the long-wave regime emerges for values of $\overline{W}_1$ and $\overline{W}_2$ not very small in comparison with one. Moreover, if the cancellation of the long-wave mode occurs due to the weakness of the induction of both the first and the second orders, which is plausible, then we cannot dismiss the possibility that the ignored terms of higher orders might play a dominant role and render our result invalid. In any event, the disappearance of the

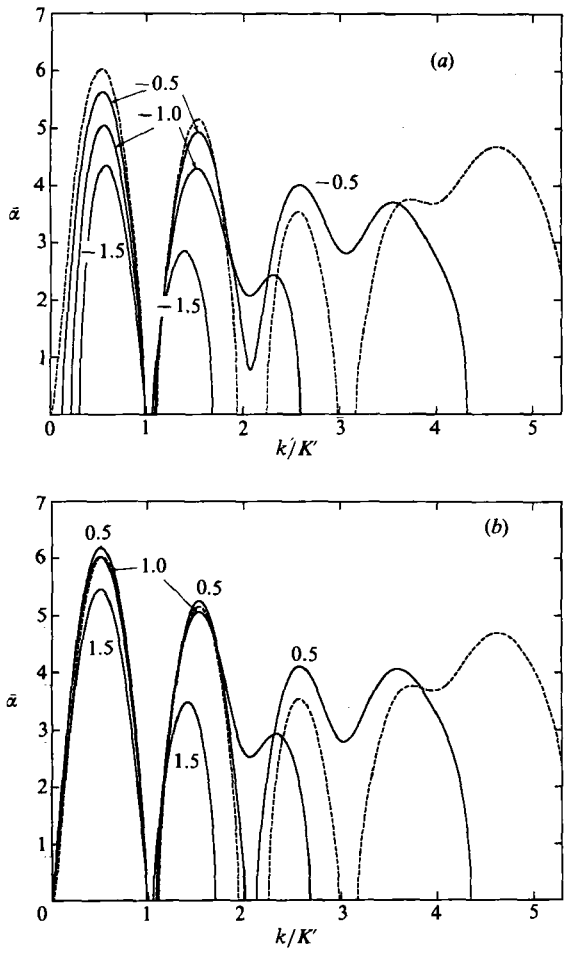

FIGURE 6. As figure 4 but with $\tan\beta = 0.2$. (*a*) $a/R = 0.33$, $W/V \leqslant 0$; (*b*) $a/R = 0.33$, $W/V \geqslant 0$.

long-wave instability mode is marginal. In the following subsection, we discuss its validity.

Keeping these limitations of the approximation in mind, we proceed to the cases of helices with smaller pitch. Figures 5(*a*) and 5(*b*) show the amplification rate for helices with $\tan\beta = 0.3$ and $a/R = 0.33$. Figures 6(*a*) and 6(*b*) exhibit the case of $\tan\beta = 0.2$ and $a/R = 0.33$. The tendency of the stabilizing or destabilizing effect of the axial flow on the long-wave mode is the same as the case of $\tan\beta = 1$. However, the non-local induction becomes stronger as the pitch decreases and the complete cancellation of the long-wave mode is unattainable.

Widnall (1972) discovered the third instability mode, called the mutual-inductance instability mode. This mode is considered to originate from the mutual inductance between the successive turns of the helix. It has a peak at $k/K' = 1.5$ for $\tan\beta = 0.3$ and has two peaks at $k/K' = 1.5$ and 2.5 for $\tan\beta = 0.2$. The cutoff model may not portray these parameter regions accurately and it is sometimes difficult to discriminate between the mutual-inductance and the short-wave modes. The general trends of this mode, we speculate, are as follows: for $a/R = 0.33$, as opposed to the long-wave mode, the addition of the negative axial velocity $W/V < 0$ makes the

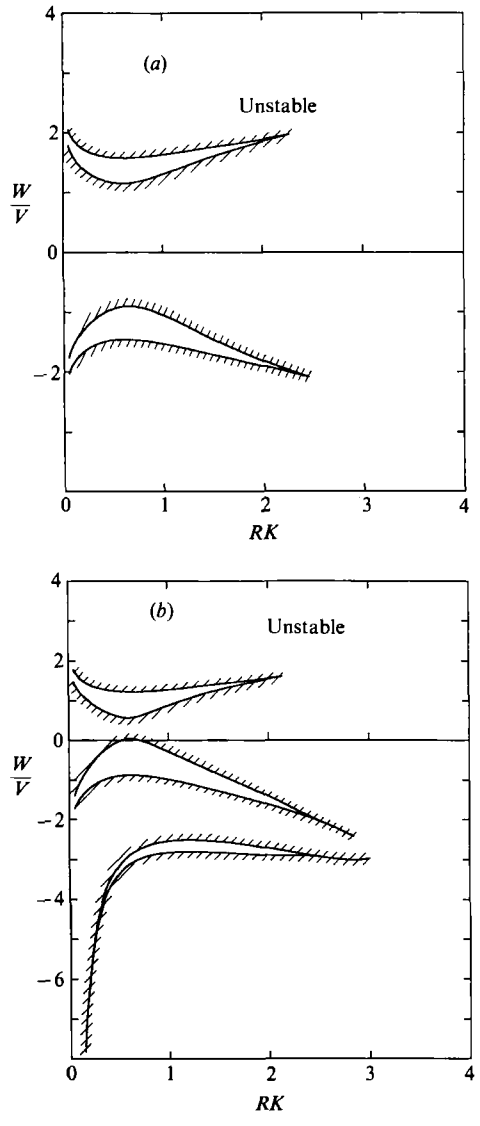

FIGURE 7. Stability boundary in the $(RK, W/V)$-plane when the long-wave instability mode wholly vanishes. Crescent-shaped areas enclosed by two arcs denote the stability regions. (*a*) $a/R = 0.1$; (*b*) $a/R = 0.3$.

amplification rate larger and at a certain negative value of W/V it merges with the short-wave mode. Below some value of W/V the resulting amalgamated mode shrinks. For $W/V \geqslant 0$, the mutual-induction mode first shrinks and later grows as the axial velocity becomes larger. The later stage is similar to the case of $W/V \leqslant 0$. The major difference between the cases of $\tan\beta = 0.3$ and 0.2 is that in the latter case the mode located in the range $1 < k/K' < 2$ begins to shrink in the presence of negative W/V small in magnitude.

In figures 7(*a*) and 7(*b*), we present the stability boundaries for the long-wave mode for various ratios $a/R = 0.1$ and 0.3, respectively. The narrow regions of a deformed crescent shape bounded by two curves designate the parameter range in which the long-wave mode is suppressed. the judgement of whether an instability

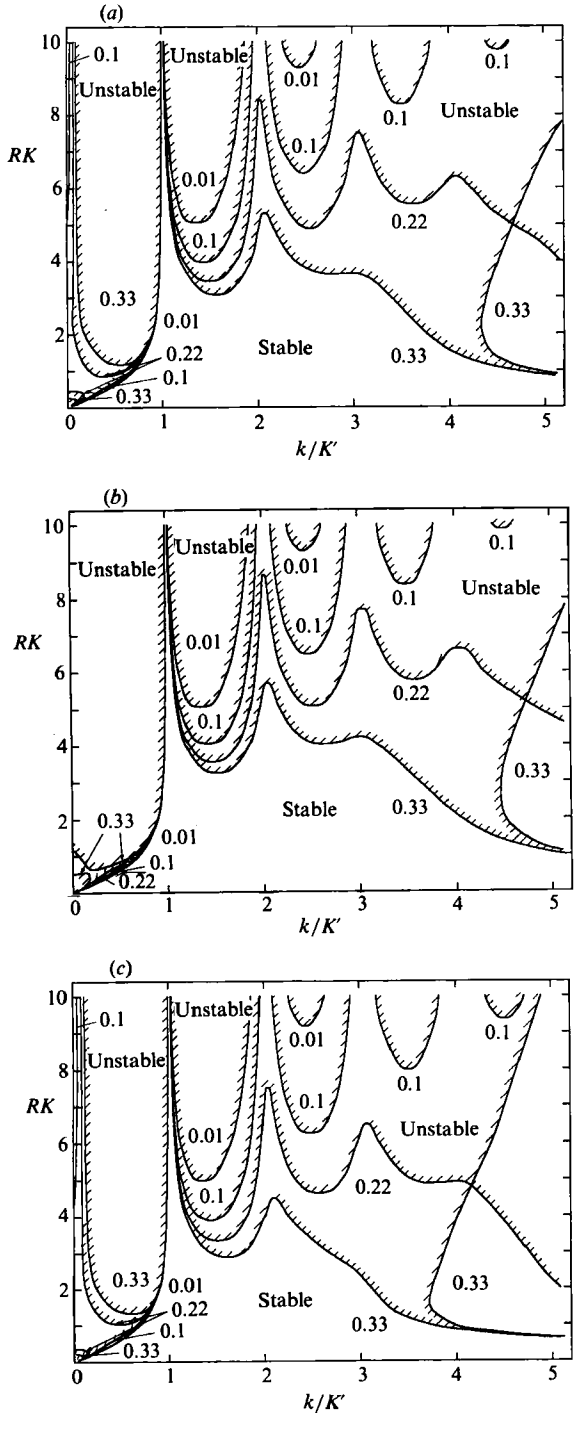

FIGURE 8. Stability boundaries in the $(k/K', RK)$-plane for a fixed W/V. The values of the ratio a/R of core to cylinder radi are indicated on each curve. Areas above the boundaries, except in the immediate neighbourhood of the origin, denote the instability regions. (*a*) Rankine's vortex as defined by (4.31) with $W/V = -0.4$; (*b*) Rankine's vortex with $W/V = 0.4$; (*c*) Burgers' vortex as defined by (2.93) and (2.94) with the parameter values given by Maxworthy *et al.* (1985).

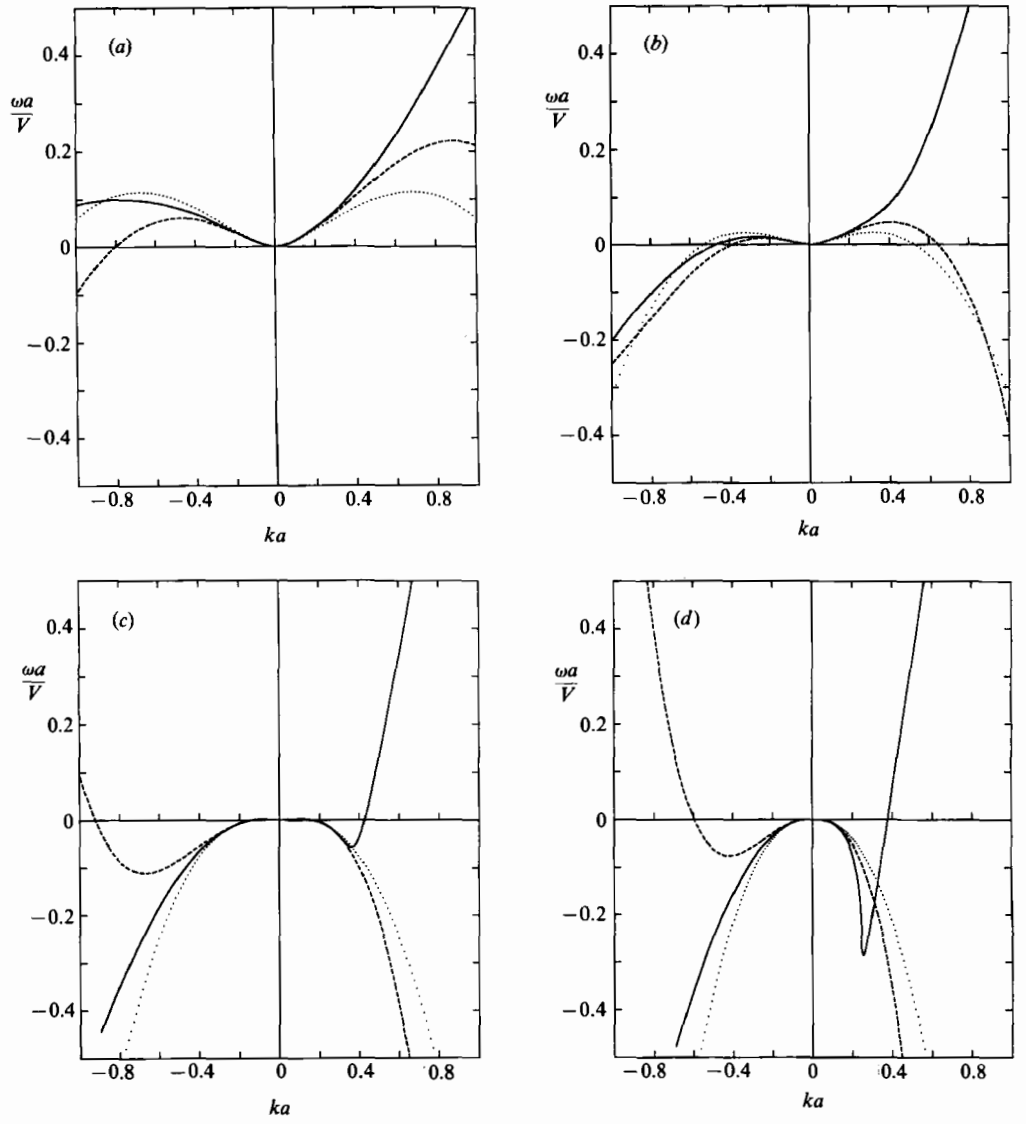

FIGURE 9. First branch of the dispersion relation for bending waves on Rankine's vortex (4.31) for different values of W/V (the ratio of axial to swirl velocity). The dashed line is the second-order formula (2.108). the dotted line is the first-order formula. (*a*) $W/V = 0.5$; (*b*) $W/V = 1.0$; (*c*) $W/V = 1.5$; (*d*) $W/V = 2.0$.

mode belongs to the long-wave mode or not is somewhat subjective around the parameter value where the long-wave mode reappears, and $\overline{W}_1$ and $\overline{W}_2$ are not very small in comparison with one in such a region. Therefore the second critical values at which the long-wave mode reappears may not always be precise. It is noted that another instability mode sometimes appears very close to the long-wave regime in the parameter range of the stability window. The stability window does not necessarily imply that the helicoidal filament is stable against all perturbations of moderate and long wavelengths.

We see from figure 7 (a) that one stability window exists on each side of negative and positive W/V. At a fixed value of RK, the window of negative W/V is closer to

the abscissa and has wider range of W/V than the positive side. As the pitch becomes smaller or the neighbouring turns gather closer, the destabilizing effect of non-local induction predominates over the stabilizing effect of axial flow so that the stability window disappears above some critical value of RK. The critical value is larger for $W/V < 0$. The extrapolation of the boundary curves toward $RK = 0$ may lead us to the suspicion that the straight vortex tube ($RK = 0$) is unstable to long-wavelength perturbations for most values of W/V. In reality, the amplification rate becomes smaller as the pitch becomes larger and it will tend to zero in the limit of $RK \to 0$. We interpret this to mean that the straight vortex is stable against long-wavelength perturbations. The remarkable feature of figure 7(*b*) is that there exist two stability windows for $W/V \leqslant 0$, though our approximation may cease to be valid in the second window because $\overline{W}_1$ and $\overline{W}_2$ are not small. Comparing figures 7(*a*) and 7(*b*), we observe that for fatter vortex cores, the band of stability occurs at values of W/V smaller in magnitude and is wider in both W/V and RK. In short, helicoidal filaments with fat cores can easily undergo stabilization by the action of axial flow, as far as the long-wave mode is concerned.

To illustrate the dependence of stability characteristics on wavenumbers, we display in figures 8(*a*) and 8(*b*) the neutral stability curve as a function of k/K' for several vortex core radii. We fix the value of the velocity ratio as $W/V = -0.4$ in figure 8(*a*) and $W/V = 0.4$ in figure 8(*b*). For the most part, the helicoidal filament of that core size is unstable above the boundary but in the small regions located close to the origin it is unstable below the boundary. We see that for a fat core, there appears a band of RK in which the long-wave instability mode is excluded. This band is possible for vortices with smaller core size and is wider, at the same value of magnitude of W/V, when $W/V < 0$ than when $W/V > 0$. As regards the mutual-inductance mode, the critical value of RK at which it first emerges for a given value of k/K' is a little smaller for $W/V = -0.4$ than for $W/V = 0.4$. It is noteworthy that the mutual-inductance as well as the long-wave modes are prohibited in the band mentioned above.

For comparison with the experiment conducted by Maxworthy *et al.* (1985), we illustrate in figure 8(*c*) the stability boundaries for velocity profiles (2.93) and (2.94) of Burgers' vortex with parameters chosen to fit data in their experiment. The global feature resembles that of Rankine's vortex with $W/V = -0.4$ (figure 8*a*). The broad band of absence of the long-wave mode is conspicuous. By using the indicated values of the geometric parameters ($RK = 0.23$ and $a/R = 0.83$), we have checked that the observed helical vortex is stable to perturbations of long wavelength.

4.3. *Discussion*

The results obtained in §4.2 are, if we limit ourselves to the long-wave instability mode, summarized as follows: the presence of axial flow within the core brings about asymmetry of stability characteristics between right- and left-handed helices. When its magnitude is not large enough, the axial velocity acts to stabilize left-handed helices and destabilize right-handed ones if the helicity is positive. For negative helicity, the opposite is true. When the magnitude is larger than some value dependent on a/R and RK, the axial velocity acts to reduce the amplification rate of helices of both senses. The suppression of the long-wave mode is established at moderate values of $|W/V|$, the critical value of which is smaller for left- (right)-handed helices if helicity is positive (negative). This property is novel. The parameter values for the occurrence of the suppression, unfortunately, appear to be marginal if we are reminded of the assumptions about the asymptotic expansions, i.e. $a\kappa \ll 1$ and

$\overline{W}_1$, $\overline{W}_2 \ll 1$. This result might be wholly due to the unreasonable truncation of the expansions.

One of the available formulae valid in the entire range of both wavelength and axial velocity is the linear dispersion relation for Rankine's vortex obtained by Krishnamoorthy (1966) and Lessen, Deshpande & Hadji-Ohanes (1973) (see also Moore & Saffman 1972), though it is applicable only to waves of infinitesimal amplitude on a straight vortex column. As is well known, the dispersion relation admits an infinite number of branches even if we confine ourselves to the bending waves. The relevant mode in question is the primary bending mode, the frequency of which vanishes at zero wavenumber. As an attempt to substantiate our prediction, we make a comparison between the exact dispersion relation of the first branch and its asymptotic formulae provided by (2.108).

Figure 9(*a–d*) displays the normalized frequency as a function of the normalized wavenumber for different velocity ratios (for $W/V = 0.5$, 1.0, 1.5 and 2.0 respectively). The dashed and dotted curves are asymptotic formulae correct to second and first orders, respectively. Apart from the case $W/V = 2.0$, the agreement is acceptable for $|k|a$ up to about 0.3, the second-order formula being closer to the exact one as expected. Roughly speaking, the window of suppression of the long-wave mode occurs for $|k|a < 0.1$, $\kappa a < 0.3$ and $|W/V| \lesssim 2.0$, except that another window appears for $|W/V| > 2.0$ when $a/R = 0.3$. In this respect, our approximation is reliable.

Even the first-order formula is not a bad approximation in the same parameter range. Calculation on the stability of the helicoidal vortex is performed using the same cutoff approximation as Widnall (1972). The only difference is that (4.8) includes a term proportional to the square of the axial velocity in our first-order model. The numerical results demonstrate that the stability window indeed exists in the first-order cutoff model also, but without the second-order terms, the axial velocity cannot detect the difference of stability between a right- and a left-handed helix and the critical value at which the window first appears is located between those for a right- and a left-handed helix in the second-order cutoff model. Hence the extension of the asymptotic expansions to second order is not essential for the existence of the stability window. But it is more accurate than the first-order one, capturing the asymmetry, and is therefore preferable.

More remarkable is that a wavenumber region in the neighbourhood of the origin appears at moderate values of velocity ratios W/V where the frequency becomes extremely small. For example, it appears to the left of the origin for $W/V = 1.0$ and on both sides of the origin for $W/V = 1.5$.

As for long or short waves on a straight vortex filament subjected to a strain field, which serves as a model for the understanding of the vortex-pair instability or of the short-wave instability on a vortex ring, the self-induced rotation of the sinusoidally perturbed filament tends to stabilize the vortex against distortion by the imposed strain (Crow 1970; Widnall *et al.* 1974; Moore & Saffman 1975). The asymptotic theory fails to describe the short-wave instability because the self-induced velocity vanishes, spuriously, at a wavenumber comparable to the core radius, which predict the spurious instability.

On the other hand, if we compare the numerical results of §4.2 with the dispersion relation, it is highly likely that the slowing down of the self-induced velocity owing to the inclusion of axial flow renders the instability weak and that the cancellation of the long-wave mode is accomplished when the induced velocity becomes quite small over the whole long-wave regime. This is not a proof but it is a natural

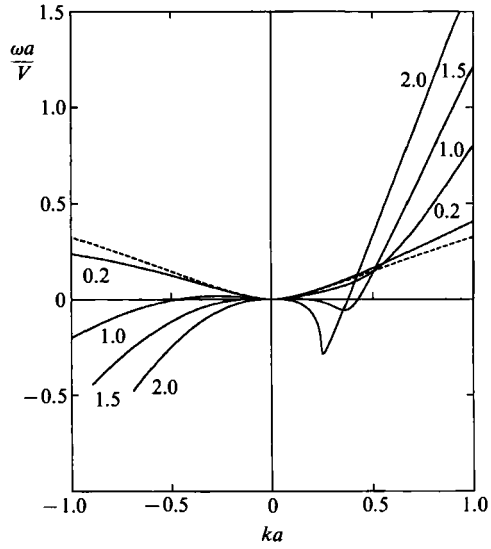

FIGURE 10. Variation of the dispersion relation of the first bending mode with W/V. The values of W/V are indicated on each curve. The dashed line corresponds to $W/V = 0$.

conclusion to draw. For example, we may refer to the fact that the amplification rate of disturbance grows as the pitch of the helicoidal filament becomes smaller and thus the self-induction is stronger. The helicoidal filament whose self-induction is quite small owing to the axial velocity may be identified with a straight vortex. It is illuminating to illustrate the variation of the dispersion relation with W/V. We show it in figure 10. The termination of the curves implies that, for short wavelengths, real frequency ceases to be allowed and is replaced by a complex root, corresponding to the Kelvin–Helmholtz instability. The variation of the frequency in the small-wavenumber range is, surprisingly, in accord with that of the amplification rate of disturbance on a helicoidal filament in the cutoff model. The curve for $W/V = 0.2$ seems to account for the destabilization of a right-handed helix and the stabilization of a left-handed helix with positive helicity. Above some value of W/V, the frequency tends to diminish with W/V for both senses of helices, reflecting the decrease of the amplification rate. The striking feature is the appearance of the wide wavenumber range on either side of origin over which the curve tangents approximately to the abscissa when $W/V = 1.5$. Incidentally, we note that the zeros of the frequency occurring closer to the origin than the exact one but belonging to short waves in the asymptotic formula for small W/V, as shown by figure 9(*a*), will be irrelevant to the existence of the stability window, because they are located outside the parameter range corresponding to the window.

The behaviour of the dispersion relation helps in understanding why the local-induction approximation is incapable of capturing the stabilization of a right(left)-handed helix with positive (negative) helicity by the action of the axial velocity. For this, it is informative to have a look at the asymptotic formula (2.108) supplemented by (2.106). The reduction of the frequency is because the constant C_1 depends on $-\log|k|$ and $-(W/V)^2$. In the localized induction approximation, however, we set C_1 merely to be a positive constant and reduce the dispersion relation to a simple third-order algebraic equation in the wavenumber, as is evident from (3.13) or (3.14). The local-induction approximation thus fails to suppress the long-wave mode of

right(left)-handed helices with positive(negative) helicity. As pointed out by Leibovich (1970) and Pritchard (1970), the logarithmic dependence of the dispersion relation on the wavenumber is due to the irrotational motion of fluid outside the vortex core in an unbounded space and the governing equation for very long waves is then superseded by a nonlinear integro-differential equation. Leibovich *et al.* (1986) derived such an equation for bending waves, though it is limited only to small perturbations on a straight columnar vortex. The construction of an integro-differential equation applicable to large-amplitude bending waves will be an interesting extension.

The asymmetric influence of the axial velocity upon helical waves on a vortex filament has already reported by Lessen, *et al.* (1973) and Lessen, Singh & Paillet (1974). Finally we comment upon the relation between our results and theirs. At first sight, our results on the stability of a helicoidal filament may seem to have much in common with those of LSP on the stability of Burgers' vortex. They deal with small-amplitude bending waves on a straight vortex with axial flow whose velocity profiles are Gaussian. A straight vortex tube is stable to long-wave perturbations, which is different from a helicoidal vortex. In fact, the bending waves of instability found by them have wavelengths comparable with the vortex core as long as the axial velocity is not very large in magnitude. This is a pronounced difference. This short-wave instability mode is analogous to the Kelvin–Helmholtz instability. It depends on the detail of the core structure, which is illustrated by the difference between Rankine's vortex studied by Lessen *et al.* (1973) and Burgers' vortex studied by Lessen *et al.* (1974). There is a discussion on this point in the paper of Lundgren & Ashurst (1989). Our study and Lessen's *et al.*'s (1973, 1974) are thus complementary to each other.

5. Conclusion

We have investigated, in this paper, the long bending distortions of a thin vortex filament with axial flow inside the vortex core. The equation of motion is derived by the method of matched asymptotic expansions up to the second order in the expansion parameter $\epsilon = a_0$ (vortex-core radius)$/R_0$ (typical radius of curvature) which is assumed to be sufficiently small. On the other hand, no restriction is placed on the wave amplitude. The resulting equation is identical to the Moore–Saffman equation. The dispersion relation for long infinitesimal waves on a Burgers' vortex is calculated to the second order. It is found that the inclusion of the second-order terms achieves a great improvement in the approximation of the dispersion relation.

If we neglect the non-local induction and the variation of the cutoff parameter L/a along the vortex filament, we can extract the new integrable equation (3.1), which is a natural generalization of the localized induction equation (1.2). This new equation is shown to be equivalent to the Hirota equation through Hasimoto's transformation.

The N-soliton solution is obtained explicitly, using the technique of the 'soliton surface approach' by Sym as well as Hirota's method of bilinear form (Miyazaki & Fukumoto 1988). The form of the solution is the same as that of the LIE, if the pertinent dispersion relation is used. The helicoidal vortex and a form of Euler's elastica are determined as examples of the vortex filament that translates and rotates steadily without changing shape. The axial-flow effect is found to modify the translation velocity and the rotation rate, leaving the distortion shape unaffected. The linear stability of a helicoidal vortex filament is studied based on the new equation. It is striking that the presence of the axial flow has a profound influence

on the stability and that a helicoidal vortex filament with the special torsion $\tau_0 = -1/(3W)$ becomes neutrally stable against any small perturbations.

In order to consolidate the prediction under the localized induction approximation, we have carried out a full calculation incorporating the effect of the entire perturbed filament. A cutoff method generalized to second-order in the curvature effect is devised to calculate the Biot–Savart integral. The numerical results show that, for the long-wave instability mode, the axial velocity W, if the ratio $|W/V|$ of its magnitude to the maximum swirl velocity V is small enough, tends to stabilize left (right)-handed helices and to destabilize right (left)-handed helices if the given helicity is positive (negative). In the range of small $|W/V|$, the prediction of the local model coincides qualitatively with that of the cutoff model. The discrepancy manifests itself as $|W/V|$ becomes larger. Above some values of $|W/V|$, the amplification rate of the long-wave mode diminishes for both right- and left-handed helices. The prohibition of the long-wave mode is established in a band of W/V, provided that the pitch of the helix is not too small. The boundary values of the stability window depend on the pitch, the core radius and the sense (torsion) of the helix. The major difference between the two models is that, in the cutoff model, the suppression of the long-wave mode can be achieved by the first-order curvature effect alone, whereas the second-order effect is essential in the local model. The neglect of core structure and the non-local induction accounts for this failure.

The authors are grateful to Professors H. Hasimoto and T. Kambe for illuminating discussions. The work of Y.F. was partially supported by a Grant-in-Aid for Scientific Research from the Ministry of Education, Science and Culture of Japan.

Appendix A. Local cylindrical coordinates and the equations of motion

In this Appendix we include the necessary formulae for the local moving curvilinear coordinate system and the equations of motion for an inviscid fluid rewritten in terms of this coordinate system. The details are contained in the paper of Callegari & Ting (1978).

As introduced in §2.2, the position vector $\boldsymbol{x}$ in the fluid is given in terms of the local cylindrical coordinates (r, θ, s) by (2.4). In this system, $\boldsymbol{e}_r = \boldsymbol{e}_r(\theta, s, t)$, $\boldsymbol{e}_\theta = \boldsymbol{e}_\theta(\theta, s, t)$ and $\boldsymbol{t} = \boldsymbol{t}(s, t)$ constitute a set of orthonormal unit vectors centred on the nearest position $\boldsymbol{X}(s, t)$ on the filament. The first two of them are given by

$$\boldsymbol{e}_r = \boldsymbol{n}\cos\varphi + \boldsymbol{b}\sin\varphi, \tag{A 1}$$

$$\boldsymbol{e}_\theta = \boldsymbol{b}\cos\varphi - \boldsymbol{n}\sin\varphi. \tag{A 2}$$

With the help of the Serret–Frenet equations (3.4), we get

$$\frac{\partial \boldsymbol{e}_r}{\partial r} = \frac{\partial \boldsymbol{e}_\theta}{\partial r} = \frac{\partial \boldsymbol{t}}{\partial r} = \boldsymbol{0}, \tag{A 3}$$

$$\frac{\partial \boldsymbol{e}_r}{\partial \theta} = \boldsymbol{e}_\theta, \quad \frac{\partial \boldsymbol{e}_\theta}{\partial \theta} = -\boldsymbol{e}_r, \quad \frac{\partial \boldsymbol{t}}{\partial \theta} = \boldsymbol{0}, \tag{A 4}$$

$$\frac{\partial \boldsymbol{e}_r}{\partial s} = -\kappa\cos\varphi\boldsymbol{t}, \quad \frac{\partial \boldsymbol{e}_\theta}{\partial s} = \kappa\sin\varphi\boldsymbol{t}, \quad \frac{\partial \boldsymbol{t}}{\partial s} = \kappa\boldsymbol{n}. \tag{A 5}$$

Now we rewrite the Euler equations and the equation of continuity. It is sometimes convenient to specify the position along the filament curve by using the marker

variable ξ instead of s, which satisfies the condition (2.17). We may employ either ξ or s as the arc-length parameter indistinguishably. The velocity $\boldsymbol{V} = (u, v, w)$ in the moving coordinate system is connected with the velocity $\boldsymbol{v}$ in the rest frame by (2.27), which is written with the dimensional variables as

$$\boldsymbol{v} = \dot{\boldsymbol{X}} + \boldsymbol{V}. \tag{A 6}$$

Here a dot denotes the time derivative with fixed r, θ and ξ. further, the coordinate transformation is accompanied by the change of the time derivative:

$$\frac{\partial}{\partial t} \to \frac{\partial}{\partial t} - (\dot{\boldsymbol{X}} + r\dot{\boldsymbol{e}}_r) \cdot \boldsymbol{\nabla}_{r\theta s}. \tag{A 7}$$

Then the Euler equations are rewritten in the moving coordinate system as

$$\ddot{\boldsymbol{X}} + \frac{1}{\sigma}(w - r\dot{\boldsymbol{e}}_r \cdot \boldsymbol{t})\,\dot{\boldsymbol{X}}_\xi + \frac{\mathrm{d}\boldsymbol{V}}{\mathrm{d}t} = -(p_r \boldsymbol{e}_r + \frac{1}{r} p_\theta \boldsymbol{e}_\theta + \frac{1}{h} p_s \boldsymbol{t}), \tag{A 8}$$

where

$$\begin{aligned}
\frac{\mathrm{d}\boldsymbol{V}}{\mathrm{d}t} = {} & \left\{ \dot{u} + w\boldsymbol{e}_r \cdot \dot{\boldsymbol{t}} + uu_r + \frac{1}{r}(v - r\dot{\boldsymbol{e}}_r \cdot \boldsymbol{e}_\theta)\, u_\theta - \frac{v^2}{r} + \frac{1}{h}(w - r\dot{\boldsymbol{e}}_r \cdot \boldsymbol{t})\,[u_s + \kappa w(\boldsymbol{n} \cdot \boldsymbol{e}_r)] \right\} \boldsymbol{e}_r \\
& + \left\{ \dot{v} + w\boldsymbol{e}_\theta \cdot \dot{\boldsymbol{t}} + uv_r + \frac{1}{r}(v - r\dot{\boldsymbol{e}}_r \cdot \boldsymbol{e}_\theta)\,(v_\theta + u) + \frac{1}{h}(w - r\dot{\boldsymbol{e}}_r \cdot \boldsymbol{t})\,[v_s + \kappa w(\boldsymbol{n} \cdot \boldsymbol{e}_\theta)] + u\dot{\boldsymbol{e}}_r \cdot \boldsymbol{e}_\theta \right\} \boldsymbol{e}_\theta \\
& + \left\{ \dot{w} + u\dot{\boldsymbol{e}}_r \cdot \boldsymbol{t} + v\dot{\boldsymbol{e}}_\theta \cdot \boldsymbol{t} + uw_r + \frac{w_\theta}{r}(v - re_r \cdot \boldsymbol{e}_\theta) + \frac{1}{h}(w - r\dot{\boldsymbol{e}}_r \cdot \boldsymbol{t})\,[w_s - (\boldsymbol{V} \cdot \boldsymbol{n})\kappa] \right\} \boldsymbol{t},
\end{aligned} \tag{A 9}$$

with h defined by (2.6):

$$h = 1 - \kappa r \cos\varphi, \tag{A 10}$$

and

$$\sigma = |\boldsymbol{X}_\xi| = \frac{\partial s}{\partial \xi}. \tag{A 11}$$

The equation of continuity becomes, for an incompressible fluid,

$$(rhu)_r + (hv)_\theta + r\left(w_s + \frac{1}{\sigma}\dot{\boldsymbol{X}}_\xi \cdot \boldsymbol{t}\right) = 0. \tag{A 12}$$

REFERENCES

Aref, H. & Flinchem, E. P. 1984 Dynamics of a vortex filament in a shear flow. *J. Fluid Mech.* **148**, 477–497.

Arms, R. J. & Hama, F. R. 1965 Localized-induction concept on a curved vortex and motion of an elliptic vortex ring. *Phys. Fluids* **8**, 553–559.

Betchov, R. 1965 On the curvature and torsion of an isolated vortex filament. *J. Fluid Mech.* **22**, 471–479.

Callegari, A. J. & Ting, L. 1978 Motion of a curved vortex filament with decaying vortical core and axial velocity. *SIAM J. Appl. Maths* **35**. 148–175.

Crow, S. C. 1970 Stability theory for a pair of trailing vortices. *AIAA J.* **8**, 2172–2179.

Fukumoto, Y. & Miyazaki, T. 1986 *N*-solitons on a curved vortex filament. *J. Phys. Soc. Japan* **55**, 4152–4155.

Fukumoto, Y. & Miyazaki, T. 1988 *N*-solitons propagating on a thin curved vortex filament. In *Proc. 36th Japan Natl Congr. for Theoretical and Applied Mechanics, 1986*; *Theoretical and applied Mechanics*, Vol. 36. Tokyo University Press.

HAMA, F. R. 1962 Progressive deformation of a curved vortex filament by its own induction. *Phys. Fluids* **5**, 1156–1162.

HAMA, F. R. 1963 Progressive deformation of a perturbed line vortex filament. *Phys. Fluids* **6**, 526–534.

HASIMOTO, H. 1971 Motion of a vortex filament and its relation to elastica. *J. Phys. Soc. Japan* **31**, 293 – 294.

HASIMOTO, H. 1972 A soliton on a vortex filament. *J. Fluid Mech.* **51**, 477–485.

HASIMOTO, H. & KAMBE, T. 1985 Simulation of invariant shape of a vortex filament with an elastic rod. *J. Phys. Soc. Japan* **54**, 5–7.

HIROTA, R. 1973 Exact envelope-soliton solutions of a nonlinear wave equation. *J. Math. Phys.* **14**, 805–809.

HIROTA, R. 1982 Bilinearization of soliton equations. *J. Phys. Soc. Japan* **51**, 323–331.

HOPFINGER, E. J., BROWAND, F. K. & GAGNE, Y. 1982 Turbulence and waves in a rotating tank. *J. Fluid Mech.* **125**, 505–534.

HOWARD, L. N. & GUPTA, A. S. 1962 On the hydrodynamic and hydromagnetic stability of swirling flows. *J. Fluid Mech.* **14**, 463–476.

KIDA, S. 1981 A vortex filament moving without change of form. *J. Fluid Mech.* **112**, 397–409.

KIDA, S. 1982 Stability of a steady vortex filament. *J. Phys. Soc. Japan* **51**, 1655–1662.

KIRCHHOFF, G. 1859 Über das gleichgewicht und die bewegung eines unendlich dünnen elastischen stabes. *J. f. Math. (Crelle), Bd.* 56.

KRISHNAMOORTHY, V. 1966 Vortex breakdown and measurements of pressure fluctuation over slender wing. Ph.D. thesis, Southampton University.

LAMB, G. L. 1977 Solitons on moving space curves. *J. Math. Phys.* **18**, 1654–1661.

LEIBOVICH, S. 1970 Weakly non-linear waves in rotating fluids. *J. Fluid Mech.* **42**, 803–822.

LEIBOVICH, S., BROWN, S. N. & PATEL, Y. 1986 Bending waves on inviscid columnar vortices. *J. Fluid Mech.* **173**, 595–624.

LEIBOVICH, S. & MA, H.-Y. 1983 Soliton propagation on vortex cores and the Hasimoto soliton. *Phys. Fluids* **26**, 3173–3179.

LESSEN, M., DESHPANDE, N. V. & HADJI-OHANES, B. 1973 Stability of a potential vortex with a non-rotating and rigid-rotating top-hat jet core. *J. Fluid Mech.* **60**, 459–466.

LESSEN, M., SINGH, P. J. & PAILLET, F. 1974 The stability of a trailing line vortex. Part 1. Inviscid theory. *J. Fluid Mech.* **63**, 753–763.

LEVI, D., RAGNISCO, O. & SYM. A. 1984 Dressing method v.s. classical Darboux transformation. *Nuovo Cim.* **83B**, 34–41.

LEVI, D., SYM, A. & WOJCIECHOWSKI, S. 1983 *N*-solitons on a vortex filament. *Phys. Lett.* **94A**, 408–411.

LEVY, H. & FORSDYKE, A. G. 1928 The steady motion and stability of a helical vortex. *Proc. R. Soc. Lond.* A **120**, 670–690.

LUNDGREN, T. S. & ASHURST, W. T. 1989 Area-varying waves on curved vortex tubes with application to vortex breakdown. *J. Fluid Mech.* **200**, 283–307.

MAXWORTHY, T., HOPFINGER, E. J. & REDEKOPP, L. G. 1985 Wave motions on vortex cores. *J. Fluid Mech.* **151**, 141–165.

MAXWORTHY, T., MORY, M. & HOPFINGER, E. J. 1983 Waves on vortex cores and their relation to vortex breakdown. In *Proc. AGARD Conf. on Aerodynamics of Vortical Type Flows in Three Dimensions*: *AGARD* CPP-342, paper 29/

MIYAZAKI, T. & FUKUMOTO, Y. 1988 *N*-solitons on a curved vortex filament with axial flow. *J. Phys. Soc. Japan.* **57**, 3365–3370.

MOORE, D. W. & SAFFMAN, P. G. 1972 The motion of a vortex filament with axial flow. *Phil. Trans. R. Soc. Lond.* A **272**, 403–429.

MOORE, D. W. & SAFFMAN, P. G. 1974 A note on the stability of a vortex ring of small cross-section. *Proc. R. Soc. Lond.* A **338**, 535–537.

MOORE, D. W. & SAFFMAN, P. G. 1975 The instability of a straight vortex filament in a strain field. *Proc. R. Soc. Lond.* A **346**. 415–425.

PRITCHARD, W. G. 1970 Solitary waves in rotating fluids. *J. Fluid Mech.* **42**, 61–83.

SAFFMAN, P. G. 1970 The velocity of viscous vortex rings. *Stud. Appl. Maths* **49**, 371–380.

SAFFMAN, P. G. 1978 The number of waves on unstable vortex rings. *J. Fluid Mech.* **84**, 625–639.

SYM, A. 1982 Soliton surfaces. *Lett. Nuovo Cim.* **33**, 394–400.

SYM, A. 1984 Soliton surfaces. VI. – Gauge invariance and final formulation of the approach. *Lett. Nuovo Cim.* **41**, 353–360.

SYM, A. 1985 Soliton surfaces and their applications. (Soliton geometry from spectral problems.) In *Geometric Aspects of The Einstein Equations and Integrable Systems* (ed. R. Martini), Lecture Notes in Physics, Vol. 239, pp. 154–231. Springer.

TSAI, C. Y. & WIDNALL, S. E. 1976 The stability of short waves on a straight vortex filament in a weak externally imposed strain field. *J. Fluid Mech.* **73**, 721–733.

WIDNALL, S. E. 1972 The stability of a helical vortex filament. *J. Fluid Mech.* **54**, 641–663.

WIDNALL, S. E., BLISS, D. B. & TSAI, C. Y. 1974 The instability of short waves on a vortex ring. *J. Fluid Mech.* **66**, 35–47.

WIDNALL, S. E., BLISS, D. B. & ZALAY, A. 1971 Theoretical and experimental study of the stability of a vortex pair. In *Proc. Symp. on Aircraft Wake Turbulence. Seattle.* Plenum.

WIDNALL, S. E. & TSAI, C. Y. 1977 The instability of the thin vortex ring of constant vorticity. *Phil. Trans. R. Soc. Lond.* A **287**, 273–305.